SLAC-PUB-1853, Revised
May 1977 (Rev.)
December 1976
(T/E)

TWO-GLUON EXCHANGE MODEL FOR ψ PHOTOPRODUCTION*

Benedikt Humpert

Stanford Linear Accelerator Center
Stanford University, Stanford, California 94305

and

Department of Theoretical Physics
University of Geneva, Geneva, Switzerland

and

A. C. D. Wright†

Stanford Linear Accelerator Center
Stanford University, Stanford, California 94305

ABSTRACT

The spin dependence of ψ photoproduction is analyzed in the context of a quark-gluon model. The ψ is treated as a non-relativistic bound state of a $c\bar{c}$ pair, with exchange of two colored vector gluons to the spinless target. Effects due to the binding of the $c\bar{c}$ pair are ignored, resulting in a simple, parameter-free model for ψ photoproduction. A detailed calculation of the helicity amplitudes and density matrix elements to leading order in s is given. The scalar gluon exchange case is also analyzed, and the decay angular distribution for $\psi \to \ell^+\ell^-$ is discussed in terms of the ψ density matrix.

(Submitted for publication.)

*Work supported in part by Energy Research and Development Administration.
†Present address: Physics Dept. and Theoretical Physics Institute, University of Alberta, Edmonton, Alberta, Canada T6G2J1.

I. INTRODUCTION

ψ photoproduction exhibits the characteristics of diffraction or Pomeron exchange, namely, an almost constant total cross section for asymptotic energies and an exponentially decreasing differential cross section. This kind of behavior was also found to hold in photoproduction of ρ, ω, and ϕ. Experimentally, the latter processes conserve s-channel helicity and, indeed, it is commonly thought that s-channel helicity conservation (SCHC) is an intrinsic characteristic of Pomeron exchange.

In previous papers[1,2] we have investigated whether SCHC also holds true for ψ photoproduction by undertaking a systematic spin analysis of various models for ψ photoproduction at asymptotic energies and near threshold. Two of the models are phenomenological parametrizations of the data for ρ photoproduction, analytically continued in the vector meson mass to $m_V = m_\psi$. Alternatively, we assumed the ψ to consist of a pair of constituents interacting with the nucleon via vector or scalar gluon exchange. The main result of this analysis is that at asymptotic energies all models predict SCHC, whereas at moderate energies, substantial violation of SCHC is possible. In particular, however, in this subasymptotic region vector gluon exchange obeys SCHC almost exactly, in contrast to the predictions of all other models.

This fact is especially significant in that the two vector gluon exchange model is perhaps the most attractive model we consider. When combined with a relativistic bound-state interpretation of the ψ, it provides a well-defined, physically reasonable "Quantum Chromodynamics"-type mechanism for photoproduction. Calculations can be carried out which are limited in precision only by the technical difficulties involved in dealing with Feynman graphs. For these reasons, we devote the bulk of the present work to a detailed examination of the two-gluon exchange picture. We include a complete discussion of the calculation of the helicity amplitudes to leading order in s, as well as detailed results for the density matrix. For a comparison of the predictions of various photoproduction models we refer the reader to Refs. 1 and 2.

The paper is organized as follows. In Section II we discuss the connection between the decay angular distribution for $\gamma N \rightarrow \psi N$ ($\psi \rightarrow e^+e^-$) and the density matrix. We consider the case of the most general ψe^+e^- coupling, and its reduction to a purely transverse coupling. The scalar and vector gluon exchange models are introduced in Section III, and calculation of the resulting Feynman graphs is discussed. Section IV presents the results of the analysis for helicity amplitudes and density matrix elements. Conclusions appear in Section V. Finally, many of the technical details of the two-gluon exchange calculation are reserved for the appendices.

II. ANGULAR DISTRIBUTION AND DENSITY MATRIX

The spin density matrix of the created vector meson V in the process $\gamma N \to VN$ determines the angular distribution of its decay products. Since $\psi \to e^+e^-, \mu^+\mu^-$ are the most important single ψ-decay modes, these can be used to determine the helicity of the created ψ-meson in the same way as the $\pi^+\pi^-$ mode in ρ-photoproduction contains information about the spin of the created ρ-meson. In this section we therefore analyze the decay angular distribution for $V \to \ell^+\ell^-$.[1]

The process we are describing is shown in Fig. 1 and its matrix element can be written as a product

$$\langle \ell^+\ell^- N_2 | T | \gamma N_1 \rangle = \langle \ell^+\ell^- | M | V \rangle \langle V | T | \gamma \rangle . \tag{2.1}$$

The first term describes the decay $V \to \ell^+\ell^-$ whereas the second is the helicity amplitude for $\gamma N \to VN$. The decay angular distribution of the vector meson in its rest frame is obtained by squaring the matrix element and summing over the helicities

$$\frac{dN}{d\cos\theta\, d\phi} \equiv W(\theta,\phi) = \sum_{VV'} \sigma_{VV'}(\theta,\phi) \cdot \rho_{VV'} . \tag{2.2}$$

Here $\rho_{VV'}$ is the spin density matrix for $\gamma N \to VN$; it is connected with the photon density matrix and the helicity amplitudes through

$$\rho_{VV'} = \sum_{\gamma\gamma'} \langle V | T | \gamma \rangle \rho_{\gamma\gamma'} \langle V' | T | \gamma' \rangle^* . \tag{2.3}$$

The above Eq. (2.1) is useful since it permits separation of the decay $V \to \ell^+\ell^-$ from the creation process $\gamma N \to VN$. Once the decay is specified it provides information on the production process by use of the decay angular distribution. Assuming that $\psi \to e^+e^-, \mu^+\mu^-$ proceeds through a photon, we have

$$\langle \ell^+\ell^- | M | V \rangle = e^2 \cdot g_V \cdot (\bar{u}_2 \gamma^\mu v_1) \cdot \epsilon_\mu(V) , \tag{2.4}$$

where g_V is the vector meson-photon coupling constant and ϵ is the vector meson-wave function. The vector meson is, of course, assumed to be on its mass shell. Once the decay mechanism is specified it is straightforward to determine

$$\sigma_{VV'}(\theta,\phi) = \sum_{\alpha} \langle V'|M|\alpha\rangle\langle\alpha|M|V\rangle , \tag{2.5}$$

where α refers to both lepton helicities. One might ask what changes would be expected if the lepton pair were directly coupled to ψ. This can easily be calculated by inserting

$$\langle \ell^+\ell^- |M|V\rangle = c_{\lambda_\alpha} \circ D^1_{\lambda_V\lambda_\alpha}(\phi,\theta,-\phi) \tag{2.6}$$

into Eq. (2.5) and by going through the same analysis with the result:

$$\sigma_{VV'} = \frac{|c_1|^2}{2} \begin{bmatrix} (1+\cos^2\theta)+2\delta\sin^2\theta & \frac{\sin 2\theta}{\sqrt{2}} e^{i\phi}(1-2\delta) & \sin^2\theta \; e^{2i\phi}(1-2\delta) \\ \frac{\sin 2\theta}{\sqrt{2}} e^{-i\phi}(1-2\delta) & 2\sin^2\theta+4\delta\cos^2\theta & \frac{-\sin 2\theta}{\sqrt{2}} e^{i\phi}(1-2\delta) \\ \sin^2\theta e^{-2i\phi}(1-2\delta) & \frac{-\sin 2\theta}{\sqrt{2}} e^{-i\phi}(1-2\delta) & (1+\cos^2\theta)+2\delta\sin^2\theta \end{bmatrix} \tag{2.7}$$

where $\delta = \left|\frac{c_0}{c_1}\right|^2$. Note that $\sigma_{VV'}$ for the photon coupling Eq. (2.4) is obtained by setting $\delta \equiv 0$, corresponding to a transverse coupling. Let us concentrate on the density matrix $\rho_{VV'}$ and go back to Eq. (2.3). So far we have not specified the form of the photon density matrix. It can be chosen in a particularly suitable form such that the photon polarization vector becomes explicit. This 'standard decomposition' is

$$\rho(V) = \rho^0 + \sum_{\alpha=1}^{3} P_\gamma^\alpha \cdot \rho^\alpha ; \tag{2.8}$$

so that the corresponding decay angular distribution reads

$$W(\theta,\phi) = W^{o}(\theta,\phi) + \sum_{\alpha=1}^{3} P_{\gamma}^{\alpha} \cdot W^{\alpha}(\theta,\phi) , \tag{2.9}$$

with the $W^{i}(\theta,\phi)$ given by[1]

$$W^{0}(\theta,\phi) = \frac{1}{2}\left(1+\rho_{00}^{0}\right) + \frac{1}{2}\left(1-3\rho_{00}^{0}\right)\cos^{2}\theta$$

$$+ \sqrt{2}\,\mathrm{Re}\,\rho_{10}^{0}\sin 2\theta\,\cos\phi + \rho_{1-1}^{0}\sin^{2}\theta\,\cos 2\phi \quad , \tag{2.10}$$

$$W^{1}(\theta,\phi) = \rho_{11}^{1}\,(1+\cos^{2}\theta) + \rho_{00}^{1}\sin^{2}\theta$$

$$+ \quad 2\,\mathrm{Re}\,\rho_{10}^{1}\sin 2\theta\,\cos\phi + \rho_{1-1}^{1}\sin^{2}\theta\,\cos 2\phi \quad , \tag{2.11}$$

$$W^{2}(\theta,\phi) = -\sqrt{2}\,\mathrm{Im}\,\rho_{10}^{2}\sin 2\theta\,\sin\phi - \mathrm{Im}\,\rho_{1-1}^{2}\sin^{2}\theta\,\sin 2\phi \quad , \tag{2.12}$$

$$W^{3}(\theta,\phi) = -\sqrt{2}\,\mathrm{Im}\,\rho_{10}^{3}\sin 2\theta\,\sin\phi - \mathrm{Im}\,\rho_{1-1}^{3}\sin^{2}\theta\,\sin 2\phi \quad . \tag{2.13}$$

III. GLUON EXCHANGE MODEL

In this section we assume the ψ to consist of a pair of heavy quarks (c-quarks) which interact via gluon exchange with the conventional SU(3)-quarks (q-quarks) of the nucleon as drawn in Fig. 2. Such a picture is natural in a quark-gluon theory of hadrons and their interactions, particularly in the case of ψ photoproduction, where quarks cannot be interchanged between the ψ and the nucleon. Furthermore, we assume that it is reasonable to retain only the lowest order, two gluon exchange graphs. This is particularly well-justified in the large -t region, where asymptotic freedom[3] arguments suggest that the quark-gluon coupling constant may be small due to the large momentum carried by the gluons. At small t, lowest order perturbation theory may not be valid, as is indicated by the diffractive t-dependence of photoproduction. Nevertheless, a two gluon exchange picture may still be tenable in this region if one invokes a quark-bag interaction to provide the exponential t dependence. This is the case in the Low-Nussinov model[4] of the Pomeron. Therefore, we consider it worthwhile to investigate the consequences of the two gluon exchange picture for the spin dependence of ψ photoproduction. Having chosen a model for the Pomeron, we now consider the nature of the ψ. Motivated by the success of the charmonium model[5] in describing the spectrum and decays of the pions, we assume that the ψ is a nonrelativistic bound state of a $c\bar{c}$ pair. Due to the large charmed quark mass, the quarks are almost free and the ψ's momentum is equipartitioned between them. Thus our model is defined by the diagrams shown in Fig. 3. In what follows, we perform the loop integrations, and develop a technique to find the asymptotic form of the helicity amplitudes. We proceed in three steps: we first perform the loop integration for the case in which all particles are scalars (for clearness of presentation), subsequently the c-quarks are taken to be fermions whereas the gluons are still treated as scalars and, finally, the gluons are taken to be vectors. The nucleon is treated as a scalar throughout. The six Feynman diagrams in Fig. 3 form the smallest set of diagrams compatible with photon gauge invariance; the exchanged gluons are not gauge invariant. Since the external particles are color singlets, the calculation is performed according to the rules for QED. The infrared problem is escaped by giving the gluons a finite mass m_G in the propagator denominator. The dependence of the results on the value of m_G is discussed in detail in Section IV.

A. All Scalars

The essential difficulty in calculating the Feynman diagrams drawn in Fig. 3 is the loop integration. It can be explicitly performed by use of Feynman parametric integrals. In Appendix A we explain the method and give details of the calculation, whereas we simply state our results here:

$$T_j = G \cdot \frac{2}{t - m_\psi^2} \qquad j = (a, b, c, d) \quad , \tag{3.1}$$

$$L_j \equiv \int_0^1 (d\alpha)^4 \, I_j(\alpha) \quad , \qquad I_j(\alpha) \equiv \frac{\delta(1 - \Sigma\alpha)}{D_j^2} \quad . \tag{3.2}$$

The index j indicates which diagram we are describing and G contains all coupling constants and i-factors appearing in the vertices and propagators, as well as factors due to the loop-integration:

$$G \equiv (-ie)(-ig)^4 (i)^5 \frac{1}{(2\pi)^4} \left(-\frac{\pi^2}{i}\right) \quad . \tag{3.3}$$

Similarly, the amplitudes for diagrams (e) and (f) read:

$$T_j = 2G \cdot L_j(s,t) \qquad j = (e,f) \ , \tag{3.4}$$

$$L_j \equiv \int_0^1 (d\alpha)^5 \, I_j(\alpha) \ , \quad I_j(\alpha) \equiv \frac{\delta(1-\Sigma\alpha)}{D_j^3} \quad . \tag{3.5}$$

D_j contains the kinematical variables s and t and differs for each diagram apart from the fact that $L_{e,f}$ involve a 5-dimensional α-integration. We identify

$$\begin{aligned} D_a &\equiv D_s(4) \ , \quad D_c \equiv D_u(4) \ , \quad D_e \equiv D_s(5) \ , \\ D_b &\equiv D_u(4) \ , \quad D_d \equiv D_s(4) \ , \quad D_f \equiv D_u(5) \ , \end{aligned} \tag{3.6}$$

where $D_s(4)$ and $D_u(4)$ have been defined in Eqs. (A.10) and (A.16); similarly, the explicit forms of $D_s(5)$ and $D_u(5)$ are given in Eqs. (A.18) and (A.23). The labels (4) and (5) refer to the loop with four and five internal lines, respectively. Therefore D(4) appears in the amplitudes of diagrams j = (a,b,c,d), whereas D(5) appears in the ones with j = (e,f). Since diagrams (b,d,f) are obtained from diagrams (a,c,e) by the exchange $p_1 \leftrightarrow -p_2$ their form is obtained by the replacement $s \leftrightarrow u$ in T_a, T_c, and T_e. Note that in this case of all-scalar particles diagrams (a) and (c) are also related by $s \leftrightarrow u$ crossing; this is no longer the case for spinning particles.

Before going over to the spinning case we discuss the analytic structure of these diagrams. Diagrams (a) and (d) possess a cut along the positive real axis of the complex s-plane whose branch point is at

$$s_{B_1} \equiv (m_N + m_\psi)^2 = 16.3 \text{ GeV}^2 . \qquad (3.7)$$

There is no cut on the negative real axis for these two diagrams. The amplitudes corresponding to diagrams (b) and (c) have correspondingly a cut on the positive real axis in the complex u-plane, which, in the complex s-plane, gives a cut along the negative axis with its branch point at

$$s_{B_2} \equiv (m_N^2 - 2m_N m_\psi - t) = -t - 4.937 \text{ GeV}^2 . \qquad (3.8)$$

A similar analysis shows that diagrams (e) and (f) possess the same cuts with the same branch points. The amplitude T_e therefore has two cuts, the conventional s-cut on the positive real axis as well as the u-cut on the negative real axis. T_e can be split up into a sum of two terms, each contributing to only the right- or only the left-hand cut. The same applies for diagram (f).

B. Scalar Gluons

In the preceding subsection we have set up the formalism for spinless particles and now go a step further by taking the quark-spin into account; the gluons are still treated as scalars. The amplitudes of the first three diagrams in Fig. 3 may be cast into the form

$$T_a = G \cdot \frac{2}{t - m_\psi^2} [\bar{u}_2 (\epsilon \cdot k' - \not{\epsilon} \not{k}) \not{V}_a v_1] , \qquad (3.9)$$

$$T_c = G \cdot \frac{2}{t - m_\psi^2} [\bar{u}_2 \not{V}_c (\not{k} \not{\epsilon} - \epsilon \cdot k') v_1] , \qquad (3.10)$$

$$T_e = 2G \circ \bar{u}_2 \not{V}_e v_1 \; , \tag{3.11}$$

and the corresponding ones for diagrams (b,d,f) are obtained by the replacement $p_1 \leftrightarrow -p_2$. The $\not{V}_j$ represent the loop integrals with an internal fermion line and are evaluated in Appendix A. They have the form

$$\not{V}_j = \int_0^1 (d\alpha)^4 \circ \not{S}_j \circ I_j(\alpha) \qquad j = (a,b,c,d) \; , \tag{3.12}$$

and their spin factors are defined by

$$\begin{aligned} \not{S}_a &\equiv \{m_c - \not{x}_1\} \; , \quad & \not{S}_c &\equiv \{m_c + \not{x}_2\} \; , \\ \not{S}_b &\equiv \{m_c - \not{x}_2\} \; , \quad & \not{S}_d &\equiv \{m_c + \not{x}_1\} \; , \end{aligned} \tag{3.13}$$

where $\not{x}_1$ and $\not{x}_2$ are defined in Eqs. (A.30) and (A.31). The loop term for diagrams (e) and (f) is a 5-dimensional integral of the form given in Eq. (3.12) (j = e,f) with the spin factors

$$\begin{aligned} \not{S}_e &\equiv \not{\epsilon} \frac{D_s}{2} + \{m_c + \not{y}_1\} \not{\epsilon} \{m_c + \not{y}_1 - \not{k}\} \; , \\ \not{S}_f &\equiv \not{\epsilon} \frac{D_u}{2} + \{m_c - \not{y}_2\} \not{\epsilon} \{m_c + \not{y}_2 - \not{k}\} \; , \end{aligned} \tag{3.14}$$

where $\not{y}_1$ and $\not{y}_2$ are defined in Eqs. (A.34) and (A.35). We are now in a position to write the sum of all diagrams with four internal lines in a compact form:

$$T_a + T_b + T_c + T_d = G \circ \frac{2}{t - m_\psi^2} \int_0^1 (d\alpha)^4 \left\{ \sum_{j=a}^{d} M_j(p,\alpha) \circ I_j(\alpha) \right\} . \tag{3.15}$$

$M_j(p,\alpha)$ contains all spin factors of diagram j, such as, for example,

$$M_a(p,\alpha) \equiv \bar{u}_2 \, [\epsilon \circ k' - \not{\epsilon}\not{k}) \not{S}_a] v_1 \; , \tag{3.16}$$

and similarly for all other diagrams j = (a,b,c,d). The $M_j(p,\alpha)$ are functions of the invariant kinematical variables s,t and $(\text{masses})^2$ and depend linearly on the integration parameters α. Insertion of the explicit forms of $\not{S}_j$ into Eq. (3.12) shows that it can be cast into the invariant expansion

$$T_{abcd} \equiv T_a + T_b + T_c + T_d = G \circ \frac{2}{t-m_\psi^2} \sum_{i=1}^{4} Q_i \circ [W_i(s)+W_i(u)] \; . \qquad (3.17)$$

Q_i contains all the spin factors, whereas W_i is a sum of α-parameter integrals. We have defined

$$\begin{aligned} Q_1 &\equiv \bar{u}_2[\epsilon\circ k' - \not\epsilon \not k)\not p_1 - \not p_1(\not k\not\epsilon - \epsilon\circ k')]v_1 \\ Q_2 &\equiv -\bar{u}_2[(\epsilon\circ k' - \not\epsilon\not k)\not p_2 - \not p_2(\not k\not\epsilon - \epsilon\circ k')]v_1 \\ Q_3 &\equiv -\bar{u}_2[(\epsilon\circ k' - \not\epsilon\not k)\frac{\not k'}{2} - \frac{\not k'}{2}(\not k\not\epsilon - \epsilon\circ k')]v_1 \\ Q_4 &\equiv \bar{u}_2[(\epsilon\circ k' - \not\epsilon\not k) + (\not k\not\epsilon - \epsilon\circ k')]v_1 \; . \end{aligned} \qquad (3.18)$$

We have calculated the matrix elements for the possible helicity combinations and list our results in Appendix B. It is straightforward to determine the W_i's, with the result

$$W_{1\ldots4}(s) = \int_0^1 (d\alpha)^4 [\alpha_2/\alpha_2+\alpha_3/\alpha_2+\alpha_3+\alpha_4/1]\circ I_s(\alpha) \; , \qquad (3.19)$$

$$W_{1\ldots4}(u) = \int_0^1 (d\alpha)^4 [\alpha_2+\alpha_3/\alpha_2/\alpha_2+\alpha_3+\alpha_4/1]\circ I_u(\alpha) \; , \qquad (3.20)$$

where the first argument in the bracket of the integrand corresponds to W_1, the second one to W_2, and so on.

We can perform the same steps for diagrams (e+f). Writing

$$\not v_1 \equiv \not k'\circ a_1 + \not k\circ a_2 + \not p_1\circ a_3 \qquad (3.21)$$

with the a_i determined by Eq. (A.34), the spin factors in Eqs. (3.14) are expanded and lead to the invariant expansion:

$$T_{ef} \equiv T_e + T_f = 2G \cdot \sum_{i=5}^{13} Q_i [W_i(s) + W_i(u)] \; . \qquad (3.22)$$

The "spin amplitudes" Q_i have been chosen as follows:

$$Q_5 \equiv \bar{u}_2[\not{k}'\not{\epsilon}\not{k}']v_1 \quad , \qquad Q_9 \equiv \bar{u}_2[\not{k}\not{\epsilon}\not{p}_1 + \not{p}_1\not{\epsilon}\not{k}]v_1 \ ,$$

$$Q_6 \equiv \bar{u}_2[\not{p}_1\not{\epsilon}\not{p}_1]v_1 \quad , \qquad Q_{10} \equiv -\bar{u}_2[\not{k}'\not{\epsilon}\not{k}]v_1 \quad ,$$

$$Q_7 \equiv \bar{u}_2[\not{k}'\not{\epsilon}\not{k} + \not{k}\not{\epsilon}\not{k}']v_1 \quad , \qquad Q_{11} \equiv -\bar{u}_2[\not{p}_1\not{\epsilon}\not{k}]v_1 \quad ,$$

$$Q_8 \equiv \bar{u}_2[\not{k}'\not{\epsilon}\not{p}_1 + \not{p}_1\not{\epsilon}\not{k}']v_1 \ , \qquad Q_{12} \equiv -\bar{u}_2[\not{\epsilon}\not{k}]v_1\, m_c \quad ,$$

$$Q_{13} \equiv \bar{u}_2[\not{\epsilon}]v_1 \ , \tag{3.23}$$

and their forms, evaluated for different spin combinations, are given in Appendix B. The invariant amplitudes read

$$\begin{aligned} W_{5-13}(s) &= \int_0^1 (d\alpha)^5 [\ldots]\cdot I_s(\alpha) \ , \\ [\ldots] &\equiv [a_1^2/a_3^2/a_1a_2/a_1a_3/a_2a_3/a_1/a_3/1/(m_c^2-D_s/2)] \ , \end{aligned} \tag{3.24}$$

where again the first argument corresponds to W_5, the second to W_6, and so on. The last argument $(m_c^2-D_s/2)$ corresponds to W_{13}. The corresponding amplitudes for the u-channel coming from diagram (f), $W_i(u)$, are defined as in Eq. (3.24) with the a_i (defined by Eq. (3.21)) determined by $\not{y}_2$ in Eq. (A.35), with D_s replaced by D_u.

Up to this point our presentation has not involved any approximations and the α-parameter integrals W_i could in principle be determined exactly. Since our investigation is mostly concerned with the behavior at large energies, we have chosen to introduce their high energy approximation. By applying the techniques of ϵ-integration or Mellin transformation we find the asymptotic forms for the invariant amplitudes W_i in T_{abcd}

$$W_1(s)+W_1(u) \overset{s\to\infty}{\Longrightarrow} \frac{i\pi}{s} f_1 + \frac{2}{s} f_2 \,,$$

$$W_2(s)+W_2(u) \Longrightarrow \frac{i\pi}{s} f_1 - \frac{2}{s} f_2 \,,$$

$$W_3(s)+W_3(u) \Longrightarrow 2\,\frac{i\pi}{s} f_1 \,, \tag{3.25}$$

$$W_4(s)+W_4(u) \Longrightarrow 2\,\frac{i\pi}{s} f_1 \,.$$

f_1 and f_2 are slowly varying t-dependent functions whose detailed forms are found in Eqs. (3.51-3.52).

In the above formalism we have not yet taken into account the fact that we intend to describe photoproduction of a spin-1 particle. The amplitudes in Eqs. (3.17-3.22) describe production of a pair of c-quarks where both are assumed to have equal 4-momentum (since binding effects are ignored in this approach). Due to parity relations between the amplitudes with different helicities, we may restrict ourselves to the photon helicity: $\lambda_\gamma = +1$ throughout. We define the helicity amplitudes for $c\bar{c}$-production as $T_c(\lambda_c\lambda_{\bar{c}};\lambda_\gamma)$ and similarly for ψ-photoproduction $T(\lambda_\psi,\lambda_\gamma)$. Then

$$T(1,1) = T_c(\tfrac{1}{2}\tfrac{1}{2};1) \,,$$

$$T(0,1) = \frac{1}{\sqrt{2}}[T_c(\tfrac{1}{2} -\tfrac{1}{2};1) + T_c(-\tfrac{1}{2}+\tfrac{1}{2};1)] \,, \tag{3.26}$$

$$T(-1,1) = T_c(-\tfrac{1}{2}-\tfrac{1}{2};1) \,.$$

We are now able to give the asymptotic form of the amplitude T_{abcd} for ψ-photoproduction which receives contributions from diagrams with four propagators in the loop only

$$T(1,1) \overset{s\to\infty}{\Longrightarrow} \sqrt{2}\cdot 8 \cdot G \;\frac{1}{t-m_\psi^2}\cdot f_2 \,, \tag{3.27}$$

$$T(0,1) \overset{s\to\infty}{\Longrightarrow} \frac{G\sqrt{-t}}{t-m_\psi^2}\left[\frac{i\pi}{s} f_1 \left\{\frac{t}{2m_c} + 5m_c + \frac{m_N^2}{2m_c}\right\} - \frac{2}{s} f_2 \left\{-\frac{t}{2m_c} + 5m_c + \frac{m_N^2}{2m_c}\right\}\right], \tag{3.28}$$

$$T(-1,1) \Longrightarrow \frac{4\sqrt{2}\ G \cdot t}{t-m_\psi^2} \cdot \frac{i\pi}{s} \cdot f_1 \ . \tag{3.29}$$

We carry out the same kind of analysis for diagrams (e) and (f). By use of the REDUCE computer program we determined the asymptotic s-dependence of the T_{ef}-amplitudes; since integrals with an α_3 in the integrand depend asymptotically only on $|s|$ we find:

$$T(1,1) \overset{s\to\infty}{<} \frac{1}{s} ,$$

$$T(0,1) \sim \frac{1}{s} ,$$

$$T(-1,1) \sim \frac{1}{s} , \tag{3.30}$$

W_8, W_9, and W_{11} all contain a multiplicative α_3; they are of nonleading order in s (see subsection D), and we neglect their contributions. However, we find that for $T(0,1)$ and $T(-1,1)$, the contributions involving Q_5, Q_7, and Q_{13} also behave like $1/s$ asymptotically. Specifically, the leading asymptotic contribution to $T(0,1)$ and $T(-1,1)$ is given by

$$T_{ef} \overset{s\to\infty}{\Longrightarrow} 2G\ [Q_5\{W_5(s) + W_5(u)\} + Q_7(\{W_7(s)+W_7(u)\} + \tfrac{1}{2}\{W_{10}(s)+W_{10}(u)\}$$
$$- \tfrac{1}{4}\{W_{12}(s)+W_{12}(u)\}) + Q_{13} \cdot \{W_{13}(s)+W_{13}(u)\}] \ . \tag{3.31}$$

Taking the Q_i and the W_i to leading order in s we find

$$T(0,1) \overset{s\to\infty}{\Longrightarrow} G \cdot \frac{i\pi}{s}\sqrt{\frac{-t}{m_c^2}}\ [m_c^2\{2h_t(\alpha_2^2) - 2h_t(\alpha_2\alpha_4) + 3h_t(1)\} - \tilde{h}_t(1)] \ , \tag{3.32}$$

$$T(-1,1) \Longrightarrow G \cdot \frac{i\pi}{s}\, t\sqrt{2}\,[h_t(\alpha_2^2) - h_t(\alpha_2\alpha_4) + \frac{h_t(1)}{2}\ ] \ , \tag{3.33}$$

where the t-dependent functions h_t are defined in (3.58). Therefore, these contributions must be added to the contributions from T_{abcd} to obtain T(0,1) and T(-1,1) in leading order. We note that the T(1,1) amplitude decreases asymptotically at least one power in s faster than T_{abcd}, although the T(0,1) and T(-1,1) amplitudes contribute to order 1/s and so compete with T_{abcd}.

C. Spin-1 Gluons

We now extend our formalism to the case of spin-1 gluons (and spin-$\frac{1}{2}$ c-quarks). However, before going into the details, we first assert gauge invariance. We cut diagrams (a+c+e) at the gluon lines and consider only the c-quark part. The sum of these diagrams does satisfy the divergence condition $k \cdot (T_a+T_c+T_e) = 0$ due to the Ward-Takahashi identity.[6] An explicit proof for the model under consideration may be constructed without difficulty.

The calculation of the amplitudes here requires investigation of the spin factors $\not{L}_j$ (or $\not{S}_j$). Evaluation of their structure for diagram (a) gives (see Appendix A)

$$\not{S}_a \equiv [\not{v}_1\not{v}_2\not{v}_3 + 2D_s(\not{v}_1+\not{v}_3) + \tfrac{1}{2}D_s\gamma_\alpha\not{v}_2\gamma^\alpha] , \tag{3.34}$$

where the $\not{v}_i$ are linear combinations of the external momenta as defined in Eqs. (A.39). The expansion coefficients (a_i, b_i, c_i) are linear functions of the integration variables and are specified in Eqs. (A.40). Since the amplitude for diagram (b) is obtained by the exchange $p_1 \leftrightarrow -p_2$, which can be absorbed in the v_i by redefining their coefficients a_i, we have: $\not{S}_b \equiv \not{S}_a(v_i)$. The v_i are fixed as in Eq. (A.39), but the functions a_i are replaced by the definitions in Eq. (A.44).

The amplitudes of diagrams (c) and (a) are connected by the exchange: $p_1 \leftrightarrow -p_2$, $m_c \rightarrow -m_c$ and an overall minus sign in the amplitude leading to: $\not{S}_c \equiv -\not{S}_a(w_i)$. The above modification is absorbed not in the a_i but in the newly defined variable $\not{w}_i$ as given in Eq. (A.43). The functions a_i are the same as for diagram (a) and are defined in Eq. (A.40). Diagram (d) is calculated analogously, $\not{S}_d \equiv \not{S}_c(w_i)$, with the $\not{w}_i$ defined in Eq. (A.43) and its coefficients a_i given by Eq. (A.44).

The spin factors of diagrams (e) and (f) are composed of three contributions:

$$\not{S}_e \equiv \not{S}_{e_1} + \not{S}_{e_2} + \not{S}_{e_3} , \tag{3.35}$$

$$\begin{aligned}
\not{S}_{e_1} &\equiv \not{\epsilon} \cdot [3D_s^2 - \frac{D_s}{2} m_c^2] + D_s [(v_2 \cdot \epsilon)\not{v}_4 + (v_3 \cdot \epsilon)\not{v}_1] - \frac{D_s}{2} [\not{v}_3 \not{\epsilon} \not{v}_2 - m_c(\not{v}_1 \not{\epsilon} + \not{\epsilon} \not{v}_4)] \\
&\quad + [(m_c^2 - \frac{D_s}{2})\not{v}_1 \not{\epsilon} \not{v}_4 + D_s \{\not{v}_1 \not{v}_2 \not{\epsilon} + \not{\epsilon} \not{v}_3 \not{v}_4\}] , \\
\not{S}_{e_2} &\equiv m_c [\not{v}_1 \not{\epsilon} \not{v}_2 \not{v}_4 + \not{v}_1 \not{v}_2 \not{\epsilon} \not{v}_4] , \\
\not{S}_{e_3} &\equiv \not{v}_1 \not{v}_2 \not{\epsilon} \not{v}_3 \not{v}_4 ,
\end{aligned} \tag{3.36}$$

where $\not{v}_i$ is a linear combination of the external momenta as defined in Eq. (A.47). The spin factor of diagram (f), $\not{S}_f \equiv \not{S}_e(v_i)$, differs only in the functions $a_i \ldots$ in v_i (apart from the replacement $D_s \to D_u$), which are given in Eq. (A.49) for diagram (e) and in Eq. (A.50) for diagram (f).

In principle it is now possible to write an invariant expansion for each diagram as was done in Eqs. (3.17) and (3.22). However, in practice this is an endless undertaking. We therefore have chosen to determine the leading order approximation of the helicity amplitudes and could easily extend this analysis to any higher orders. By symbolic computing we have determined the first two terms of the spin factors dominating for asymptotic s-values. We write

$$T_j = G \cdot \frac{2}{t - m_\psi^2} \int_0^1 (d\alpha)^4 \, M_j(p,\alpha)\, I_j(\alpha) \quad j = (a,b,c,d) , \tag{3.37}$$

where

$$M_a(p,\alpha) \equiv \bar{u}_2 [(\epsilon \cdot k' - \not{\epsilon} \not{k}) \not{S}_a] v_1 , \tag{3.38}$$

$$M_c(p,\alpha) \equiv \bar{u}_2[\not{S}_c(\not{k}\not{\epsilon} - \epsilon\cdot k')]v_1 . \tag{3.39}$$

The same definitions hold for M_b (M_d) which differ from M_a (M_c) only in the expansion coefficients of the v_i(w_i) apart from changing D_s into D_u. The analogous form applies for diagrams (e) and (f)

$$T_j = 2\cdot G\cdot \int_0^1 (dx)^5 M_j(p,\alpha)\, I_j(\alpha) , \tag{3.40}$$

with

$$M_e(p,\alpha) \equiv \bar{u}_2(\not{S}_{e_1} + \not{S}_{e_2} + \not{S}_{e_3})v_1 \equiv M_{e_1} + M_{e_2} + M_{e_3} . \tag{3.41}$$

The leading order contributions of the matrix elements $M_j(p,\alpha)$ have been evaluated by a symbolic computing program for the spin combinations

$$\lambda_\gamma = +1, \qquad \lambda_c = \pm\tfrac{1}{2}, \qquad \lambda_{\bar{c}} = \pm\tfrac{1}{2} . \tag{3.42}$$

All amplitudes $M_j(p,\alpha)$ ($j = a,b,c,d$) may then be expressed in the form:

$$\begin{aligned} M_j(++) &= s \cdot (\xi_1 \ldots \xi_5) , \\ M_j(-+) &= \sqrt{\frac{-t}{m_c^2}} \cdot s \cdot (\eta_1 \ldots \eta_5) , \\ M_j(--) &= t \cdot (\zeta_1 \ldots \zeta_5) , \end{aligned} \tag{3.43}$$

where

$$(\xi_1 \ldots \xi_5) \equiv s\cdot\xi_1 + t\cdot\xi_2 + m_c^2\cdot\xi_3 + m_N^2\cdot\xi_4 + D\cdot\xi_5 . \tag{3.44}$$

The expansion coefficients ξ, η, ζ are linear combinations of products of the integration variables α and $D \equiv D(\alpha)$ is familiar from the 'all-scalar case' and reduces the power in the denominators of $I(\alpha)$. Our notation is as follows: $M_a(\pm,\pm)$ is the matrix element Eq. (3.43) of diagram (a). The helicity of the c-quark (wave function $\bar{u}_2$) is indicated in the first argument, whereas the second argument refers to the helicity of the $\bar{c}$-quark (wave function v_1). We do not consider it useful to write down all functions (ξ, η, ζ)(which differ for each diagram and each spin combination) but list in Appendix C those which are important for later arguments.

In the same way we have evaluated the asymptotic forms of the amplitude M_e as given in Eq. (3.41) and found:

$$M_{e_1}(++) = \{m_c^2 \cdot (\xi_1 \ldots \xi_4) - D_s(\xi_5 \ldots \xi_8)\} ,$$

$$M_{e_1}(-+) = \sqrt{\frac{-t}{m_c^2}}\{m_c^2(\eta_1 \ldots \eta_4) - D_s(\eta_5 \ldots \eta_8)\} ,$$

$$M_{e_1}(--) = \{m_c^2 \zeta_1 \qquad - D_s \zeta_2\} , \tag{3.45}$$

$$M_{e_2}(++) = s \cdot (\xi_1 \ldots \xi_4) ,$$

$$M_{e_2}(-+) = \sqrt{\frac{-t}{m_c^2}}\, m_c^2 \cdot (\eta_1 \ldots \eta_4),$$

$$M_{e_2}(--) = t \cdot (\zeta_1 \ldots \zeta_4) , \tag{3.46}$$

$$M_{e_3}(++) = s \cdot (\xi_1 \ldots \xi_4) ,$$

$$M_{e_3}(-+) = \sqrt{\frac{-t}{m_c^2}}\, s \cdot (\eta_1 \ldots \eta_4) ,$$

$$M_{e_3}(--) = t \cdot (\zeta_1 \ldots \zeta_4) , \tag{3.47}$$

where

$$(\xi_1 \ldots \xi_4) = s \cdot \xi_1 + t \cdot \xi_2 + m_c^2 \cdot \xi_3 + m_N^2 \cdot \xi_4 . \tag{3.48}$$

The functions $\xi_i, \eta_i, \ldots$, etc., are linear combinations of products formed by the integration parameters and differ for each diagram and contribution. For ease of notation we have dropped the index referring to the diagram or specific contribution. Each should therefore carry this index, as, for instance, $\xi_i \equiv \xi_i(e_1;\vec{\alpha})$ or $\eta_i \equiv \eta_i(a;\alpha)$, and so on. Some of the functions ξ_i, η_i, and ζ_i are listed in Appendix C. The same results hold for diagram (f), which, however, has different functions (ξ, η, ζ).

Before discussing further approximations we would like to stress that the amplitudes $M_a \ldots M_f$ given in Eqs. (3.43) and (3.45) – (3.47) are leading order approximations in the spin factors for asymptotic s-values. The invariant amplitudes have so far been treated exactly leading to integrals of the form

$$J(\xi) \equiv \int_0^1 (d\alpha)^n \cdot \xi(\alpha) \circ I(\alpha) \quad (n = 4,5) \tag{3.49}$$

whose asymptotic form will be considered in the following step.

D. Asymptotic Form of Feynman Parameter Integrals

The integrals $J(\xi)$ can in principle be calculated exactly. However we have chosen to determine their leading asymptotic behavior. Mellin transform techniques can be used in order to determine the first, second,... correction terms.[7] One might question whether such an approximation is justified at energies just above the threshold rise. In order to gain some insight we have calculated for some integrals their asymptotically leading contribution as well as their first correction terms and find in all cases that for $s \gtrsim 30\ \text{GeV}^2$ a leading order approximation gives the correct order of magnitude of the integrals although the correction terms are not yet entirely negligible.

In what follows, we present the asymptotic behavior of the integrals arising in the case of scalar gluon exchange. The evaluation of diagrams (a-d) requires the asymptotic forms of the integrals $W_{1\ldots4}(s)$ in Eq. (3.19) and similarly of $W_{1\ldots4}(u)$ in Eq. (3.20), which are easily found by use of ϵ-integration techniques.[8] The result is

$$J(\xi) \xrightarrow[s\to\infty]{} \begin{cases} \dfrac{\ell n(-\frac{s}{2})}{(+\frac{s}{2})} \cdot f_t(\xi) \text{ for } \xi \equiv \{1,\alpha_2,\alpha_4\} \\ \dfrac{1}{(+\frac{s}{2})} \quad f_t(\xi) \text{ for } \xi \equiv \{\alpha_3\} , \end{cases} \tag{3.50}$$

where the t–dependent functions $f_t(\xi)$ are

$$f_1 \equiv f_t(1) = 2f_t(\alpha_2) = 2f_t(\alpha_4) = \int_0^1 (d\alpha)^2 \frac{\delta(1-\Sigma\alpha)}{[d_s^o]} = -\frac{2}{t\cdot\delta}\ell n\left|\frac{1-\delta}{1+\delta}\right|^2 \tag{3.51}$$

with

$$\delta \equiv \sqrt{1-\frac{4m_G^2}{t}} ,$$

$$f_2 \equiv f_t(\alpha_3) = \int_0^1 (d\alpha)^3 \frac{\delta(1-\Sigma\alpha)}{[d_s^1]} = \int_0^1 dy\, \frac{1}{\delta}\,\ell n\, \frac{\delta+t(1-y)}{\delta-t(1-y)}^2 \tag{3.52}$$

with

$$\delta \equiv [t^2(1-y)^2 - 4t\{ym_N^2 + (1-y)m_G^2\}]^{\frac{1}{2}} .$$

The integrals arising in the invariant amplitudes of diagrams (e) and (f) are $W_{5\ldots13}(s)$ and $W_{5\ldots13}(u)$ as defined in Eqs. (3.24). Insertion of the explicit form for $D_j(5)$ from Eqs. (A.18) and (A.23) shows that these integrals have two cuts; one is along the positive real axis and the other is along the negative real axis. By use of the following transformation we were able to separate the two pinching singularities in the integrand and to reexpress the resulting integrals as a sum of two terms where each contains only one cut. The transformation is

$$\begin{aligned} \bar{\alpha}_5 &= \alpha_5 - \alpha_1 , \\ \bar{\alpha}_1 &= \alpha_5 + \alpha_1 , \end{aligned} \qquad \left|\frac{\partial(\alpha_1,\alpha_5)}{\partial(\bar{\alpha}_1,\bar{\alpha}_5)}\right| = \frac{1}{2} . \tag{3.53}$$

Note that the integration range is limited to the shaded region in Fig. 4. Accordingly the integrals arising in Eq. (3.24) can be written as

$$J(\xi) = \frac{1}{2}\int (d\bar{\alpha})^5 \; [(\ldots\bar{\alpha}_5\ldots) + (\ldots -\bar{\alpha}_5\ldots)] \; , \qquad (3.54)$$

where $(\ldots\alpha_5\ldots)$ is a shorthand notation for the integrand after introducing the above transformation and the convention of writing

$$\int (d\bar{\alpha})^5 \equiv \int_0^1 d\bar{\alpha}_1\ldots d\alpha_4 \int_{-\bar{\alpha}_1}^{+\bar{\alpha}_1} d\bar{\alpha}_5 \qquad (3.55)$$

is introduced. Each of the contributions in Eq. (3.54) has only one cut. The asymptotic behavior can therefore be determined by use of Mellin transformation. Straightforward application of this method to integrals with

$$\xi = \{1, (\alpha_2-\alpha_4), \alpha_4(\alpha_2-\alpha_4), (\alpha_2-\alpha_4)^2\} \qquad (3.56)$$

gives

$$J(\xi) \overset{s\to\infty}{\Longrightarrow} -\frac{i\pi}{2s}\, h_t(\xi) \qquad (3.57)$$

with

$$h_t(\xi) \equiv \int_0^1 (d\bar{\alpha})^3 \xi \frac{\delta(1-\Sigma\alpha)}{[d_s^o]^2} \; . \qquad (3.58)$$

All other contributions with $\xi = \alpha_3 \cdot (\ldots)$ were found to contribute asymptotically at least one power less in s.

We find it useful to make a few comparative remarks about the functions $f_t(\xi)$ and $h_t(\xi)$ concerning their size, t-dependence, and m_G-dependence, which will be of use for our discussion in Section V.

(i) In order to illustrate the size and t-dependence of the functions f_t (h_t) we give in Fig. 5 (Fig. 6) their t-dependence with the masses fixed at m_V = 3.1 GeV and m_G = 1.0 GeV. One notices that the size of f_t and h_t

diminishes if more integration parameters α appear in ξ and that the t-dependence is flat.

(ii) In Fig. 7 we show variation of these integrals with decreasing gluon mass. $f_t(1)$ and $h_t(1)$ both increase rapidly due to the infrared singularity.

(iii) There is no m_V-dependence in the integrals $f_t(\xi)$ whereas the integrals $h_t(\xi)$ decrease with increasing vector meson mass since the factor $1/(t-m_V^2)$ is hidden; this becomes apparent in the limit $m_G \to 0$ (Fig. 8).

The integrals $J(\xi)$ appearing in the case of spin-1 gluons for diagrams (a-d) are of similar structure to those discussed above in Eq. (3.50). Integrals with no α_1 or α_3 follow the asymptotic behavior of Eq. (3.50) whereas integrals with $\alpha_1^n \cdot (\ldots)$ or $\alpha_3^n \cdot (\ldots)$ behave asymptotically similarly to Eq. (3.50) with modified functions $f_t(\xi)$ and $h_t(\xi)$, of course. Integrals with $\alpha_1 \cdot \alpha_3$ in the integrand do not appear. The size, mass- and t-dependence of these integrals is similar to the ones discussed above. However in this case of spin-1 gluon exchange there appear new integrals of the form

$$\tilde{J}(1) \equiv \int_0^1 (d\alpha)^4 \, \frac{\delta(1-\Sigma\alpha)}{[D_s]} \xrightarrow{s\to\infty} \frac{\ell n^2(-\frac{s}{2})}{s} . \qquad (3.59)$$

The D in the denominator appears with one power less here, which is due to the multiplicative D in the expansion (3.44). If the ϵ-integration method is used in order to determine the asymptotic form, it is advantageous to use Spence functions and their asymptotic behavior. For those who prefer to apply the Mellin transformation we mention that the singularity in the integrand arises in the factor $\left(\frac{1}{A^{3+\beta}}\right)$. Similarly one can show that

$$\tilde{J}(\alpha_3) \xrightarrow{s\to\infty} \frac{\ell n(-\frac{s}{2})}{(\frac{s}{2})} . \qquad (3.60)$$

IV. FEATURES OF THE SPIN ANALYSIS

In this section, we continue our detailed analysis of the set of Feynman diagrams shown in Fig. 3, and present results of a numerical study of the helicity amplitudes and density matrix elements. Some numerical results for the density matrix have been given in Ref. 2 and have been compared with the predictions of a variety of models; here we wish to analyze the two gluon exchange picture in more detail, with emphasis on the gluon and vector meson mass dependence of the amplitudes. We first comment on the amplitudes describing vector gluon exchange between spin-$\frac{1}{2}$ quarks and a spinless nucleon. The spin part of the amplitudes $T_a \ldots T_f$ is contained in the $M_j(p,\alpha)$. Their structure is the same for all diagrams (a-d) as given in Eqs. (3.43), and in Eqs. (3.45) - (3.47) for diagrams (e) and (f). The difference for each diagram arises only through the α-dependent functions (ξ_i, η_i, ζ_i).

We consider first the loop diagrams with 4 internal lines, $j = (a,b,c,d)$. In principle we should give the explicit forms of all functions $\xi(\alpha)\ldots$. Due to limitation of space we list those which are relevant for our discussion in Appendix C. The fact that $D_a = D_d$ and $D_b = D_c$ leads us to consider the sums (M_a+M_d) and (M_b+M_c) in order to spot cancellations. Let us examine the details:

1. A superficial look at Eqs. (3.43) might lead one to the incorrect conclusion that some of the amplitudes grow like s^2. Integration over the α-parameters introduces at least a factor $1/s$. Since there are no cancellations the amplitudes $M_j(++)$ indeed grow like s^1 (if $\ell n\, s$ terms are ignored). In the sum T_{abcd}, the real part $\propto \ell n\, s$ vanishes in leading order, and the dominant contribution is purely imaginary.

2. The leading contributions to $M_j(-+)$ cancel in the sums since

$$\eta_1(a) = -\eta_1(d), \quad \eta_1(b) = -\eta_1(c) \tag{4.1}$$

as a quick look at Appendix C shows. Therefore

$$M(-+) \overset{s\to\infty}{\Longrightarrow} s^{0} . \qquad (4.2)$$

3. In $M_j(--)$, the ξ_1-terms do not entirely cancel so that M(--) is asymptotically of the same order in s as M(-+); however, numerical calculations show that for asymptotic s-values $M(--) \ll M(-+)$ because of the size of the t-dependent functions $f_t(\xi)$.

4. $M_j(++)$ contains a term $\xi_5 \equiv \{8-3\alpha_3\}$ which is multiplied by D. The resulting integral behaves asymptotically as

$$J(\xi_5) \equiv \int_0^1 (d\alpha)^4 (8-3\alpha_3) \frac{\delta(1-\Sigma\alpha)}{D_s} \overset{s\to\infty}{\Longrightarrow} \frac{[\ell n(-\frac{s}{2})]^2}{(-\frac{s}{2})} \cdot f_t \qquad (4.3)$$

and substantially enhances $M_j(++)$ due to the $\ell n^2 s$-term. Similar terms in M(-+) and M(--) are much less influential.

5. We point to the explicit m_c dependence in $M_j(-+)$ which tends to suppress this amplitude for increasing values of m_c. There is further m_c-dependence hidden in the expansion coefficients $\xi_1 \ldots$ which, however, is present in all amplitudes and is of less importance for the spin characteristics. We will elaborate more on these questions in the numerical discussions.

We now consider the amplitudes containing the loop over five internal lines. For computational convenience we have split the amplitudes into three parts:

$$\begin{aligned} M_e(p,\alpha) &\equiv M_{e_1} + M_{e_2} + M_{e_3} , \\ M_f(p,\alpha) &\equiv M_{f_1} + M_{f_2} + M_{f_3} , \end{aligned} \qquad (4.4)$$

and now discuss their properties. In Appendix C we give the explicit forms of the relevant functions ξ_i, η_i, ζ_i. Inspection of Eqs. (3.45) - (3.47) leads us to the following conclusions:

1. The contributions due to ξ_1 in $(T_{e_1} + T_{f_1})$ do not cancel due to the α_5-integration and $\xi_1(e_1) = -\xi_1(f_1)$. There is a nonvanishing contribution due to η_1.

2. $M_{e_1}(++)$ (and $M_{e_1}(--)$) possess a multiplicative m_c^2-dependence and thus grow for increasing quark masses, whereas $M_{e_1}(-+)$ is less affected.

3. The dominant contribution to diagrams (e) and (f) comes from $(T_{e_2}+T_{f_2})$ since $\xi_1(e_2) = \xi_1(f_2)$ and the asymptotic behaviors of the Feynman parameter integrals $J(\xi)$ for diagrams (e) and (f) are identical. Again, the dominant contribution is purely imaginary, but has opposite phase to the dominant contribution from T_{abcd}.

4. One notices that $M_{e_2}(++)$ has no explicit m_c-dependence; we have numerically verified that the integrals $J(\xi)$ show a strong decrease as m_c^2 increases. Therefore, to leading order diagrams (e) and (f) decrease as m_c^2 grows.

5. The contribution $(T_{e_3}+T_{f_3})$ seemingly leads to an s^2-type increase. However ξ_1 is proportional to α_3 which leads, as we show in Appendix C, to a decrease $J(\xi_1) \sim 1/s^2$; in addition there are cancellations.

6. $M_{e_3}(-+)$ seemingly rises like s^1 in the asymptotic region. However $\eta_1(e_3)$, given in Appendix C, shows that most contributions are proportional to α_3, which leads to the integral $J(\alpha_3) \sim 1/s^2$. The remaining term A_0 depends on $(\alpha_2 - \alpha_4)$. One can show that asymptotically the integrals over α_2 and over α_4 cancel since d_s^o is symmetrical under the exchange of α_2 and α_4. The same applies for the integral with $\alpha_2 \cdot \alpha_5$ as part of the integrand. We conclude that $M_{e_3}(-+) \xrightarrow{s\to\infty} s^o$.

Our second comment concerns the m_G-dependence of the density matrix element ρ_{00}^0 for vector gluon exchange. In our analysis we noticed that the amplitudes depend substantially on the gluon mass, which leads us to further investigate the m_G-dependence of ρ_{00}^0. Taking $t = -0.2$ (GeV/c)^2, we show this dependence for ρ and ψ photoproduction in Fig. 9. The same results are plotted at $t = -2.0$(GeV/c)^2

in Fig. 10. In each case there is a sharp bump in ρ_{00}^{0} at a particular gluon mass. The position and height of the bump change when m_V and/or t are varied. At low t, the peaks for ρ and ψ are of about the same height, as is the case for m_V lying between the ρ and ψ mass. At $t = -2.0\ (GeV/c)^2$ the ρ peak is much higher than the ψ peak. At small t, as m_V is decreased, the bump occurs at smaller values of m_G. This is illustrated in Fig. 11, where the position of the peak is plotted in the m_G-m_V plane for $t = -0.2\ (GeV/c)^2$.

To reveal the origin of this dramatic behavior, we plot in Fig. 12 the amplitudes T(1,1) and T(0,1) versus m_G for ψ photoproduction at $t = -0.2\ (GeV/c)^2$. This shows that Im T(1,1) has a zero at $m_G = 0.55$ GeV. Therefore, $|T(1,1)|$ is reduced at this point and $\rho_{00}^{0} \approx |T(0,1)|^2/|T(1,1)|^2$ is enhanced. The vanishing of Im T(1,1) is due to a cancellation between Im T(1,1) of diagrams (a-d) and Im T(1,1) of diagrams (e+f), which are plotted in Fig. 13. Since Im $T(1,1)_{ef}$ $\approx$ -Im $T(1,1)_{abcd}$, the resulting nonflip amplitude $|\text{Im } T(1,1)|$ is much smaller than either of its component amplitudes.

To analyze this phenomenon further, we note that for both $T(1,1)_{abcd}$ and $T(1,1)_{ef}$ terms involving the invariant integrals $f_t(1)$ and $h_t(1)$ dominate (see Figs. 5,6); of course other terms contribute as well, but they are smaller. Therefore, we examine the behavior of the functions $f_t(1)$ and $h_t(1)$. In Fig. 7 we exhibit the m_G-dependence of $f_t(1)$ and $h_t(1)$ for $t = -0.2\ (GeV/c)^2$. This behavior is mirrored in the nonflip amplitudes (Fig. 13) and the general result that $T(1,1)_{ef} \approx -T(1,1)_{abcd}$ is a consequence of the sign and magnitude of these integrals. The detailed pattern of cancellation in Im T(1,1) is governed by these terms, and also, to a lesser extent, by the other terms in the invariant expansion of the amplitude.

When the gluon mass is of the same order of magnitude as the other variables s, t, m_V^2, m_N^2 in the problem (i.e., $m_G \to 1$ GeV) the behavior of $f_t(1)$ and $h_t(1)$ is complicated. In the limit $m_G \to 0$, f_t and $h_t \propto \ln(m_G^2)$ as might be guessed from Fig. 7,

$$f_t \overset{m_G \to 0}{\approx} \frac{2}{-t} \ln(m_G^2) + (\text{finite terms}) , \tag{4.5}$$

$$h_t \overset{m_G \to 0}{\approx} \frac{2}{-t} \frac{1}{(\frac{t}{4} - m_c^2)} \ln(m_G^2) + (\text{finite terms}) . \tag{4.6}$$

It is easy to show that the contributions of these terms to the nonflip amplitude cancel (apart from the finite terms) in the limit $m_G \to 0$, so that there is no $\ln(m_G^2)$-type divergence in the overall amplitude.

In Figs. 9 and 10 we saw that the position of the bump in ρ_{00}^0 depends on t. This suggests that, for certain values of m_G, the t-dependence of ρ_{00}^0 might exhibit unexpected behavior. As an example of such behavior we show in Fig. 14 the t-dependence of ρ_{00}^0 for ρ-photoproduction at $m_G = 0.045$ GeV. Note that this value of m_G is in the region of the peak at $t = -0.2$ (GeV/c)^2 (Fig. 9). Fig. 14 shows that the expected peak is quite narrow in t, and represents a significant deviation from the general behavior of ρ_{00}^0. Again, the position of the peak depends on m_G, so that the t-dependence of ρ_{00}^0 could, in principle, be used to determine m_G.

As the vector meson mass increases, peaks in the t-dependence of ρ_{00}^0 become broader. In Fig. 15 we show ρ_{00}^0 for ψ photoproduction with $m_G = 1$ GeV. There is a broad enhancement centered at $t = -2.0$ (GeV/c)^2, after which ρ_{00}^0 resumes its usual monotonic t-dependence. Again, this effect is rather sensitive to the value of m_G, so that the results presented in Figs. 14 and 15 should be regarded as illustrative of the kind of behavior that can be expected in this model.

We conclude this section with some comments on the results described above. Since ψ photoproduction is not an elastic process, the indefinite sign of Im T(1, 1) does not necessarily imply a violation of unitarity. Note, however, that gluon gauge invariance is violated due to the use of a nonzero gluon mass. Since gauge invariance and unitarity are intimately connected it may be that violation of gluon gauge invariance manifests itself by flipping the sign of Im T(1, 1) when m_G becomes of the order of the other masses in the problem. We resorted to a study of the massive case because of the difficulty of carrying out calculations in the infrared limit.

The main result of our analysis, which appears to hold for all values of the gluon mass, is that helicity conservation is almost perfectly satisfied for ψ photoproduction even near threshold. For ρ photoproduction, the results of the model defined in Fig. 3 probably require more modification due to the more relativistic nature of the bound state. Furthermore, quark interchange diagrams can also contribute in this case. For these reasons we have not presented any comparison of our results for ρ photoproduction with the data. On the other hand, the data[9] are consistent with SCHC violation of 10% or less, in agreement with our qualitative results.

V. CONCLUSION

By combining the two-vector-gluon exchange model of the Pomeron with the nonrelativistic bound state picture for the ψ, we have obtained a simple, calculable model for ψ photoproduction. It corresponds to the simplest set of QCD diagrams consistent with photon gauge invariance. We have proceeded on the assumption that this model should provide a reasonably accurate description of the spin dependence of ψ photoproduction, and have investigated its consequences in considerable detail.

Asymptotically, this picture provides SCHC, as do all acceptable models of photoproduction. It therefore becomes necessary to study the model in the threshold region in order to distinguish its predictions from those of other models. Unfortunately, the necessity of evaluating a loop integral precludes the possibility of obtaining analytic results in this region. However, by expanding the amplitudes in powers of s, we have obtained results for the density matrix elements which we expect to be reliable fairly near threshold. Much of the paper is devoted to a detailed discussion of the techniques we have applied to the calculation of the amplitudes.

The main conclusion to be drawn from our analysis is that two vector gluon exchange conserves helicity to a very good approximation even near threshold. The amount of SCHC violation depends quite sensitively on the gluon effective mass, although it is never greater than 10% in ρ^0_{00} for ψ photoproduction. Other models which satisfy SCHC asymptotically predict a measurable helicity flip near threshold,[2] in contrast to the two vector gluon exchange model. When data on the spin dependence of ψ photoproduction become available, it will be possible to test the predictions of the various models, and in particular to confirm or rule out the simple QCD picture studied here.

ACKNOWLEDGEMENTS

We would like to thank Hannu Miettinen, Fred Gilman, and Stan Brodsky for clarifying discussions. One of us (B. H.) thanks the Swiss National Science Foundation for financial support, and the other (A. C. D. W.) acknowledges support from the National Research Council of Canada in the form of an NRC Fellowship. Both of us wish to acknowledge the warm hospitality of Professor S. D. Drell and SLAC.

APPENDIX A

This appendix gives details of the loop integration discussed in Section III. For clarity of presentation we first treat the Feynman diagrams in Fig. 4 for the case of all-scalar particles. Subsequently we generalize to spin-$\frac{1}{2}$ c-quarks (keeping the gluon spin 0) and finally we consider the case of spin-$\frac{1}{2}$ c-quarks interacting via spin-1 gluons with the spinless nucleon. We first list a few integrals which will be of later use:

$$I_0 \equiv \int_{-\infty}^{+\infty} \frac{d^4\ell}{[A \pm \ell^2]^\lambda} = \frac{i\pi^2}{(\lambda-1)(\lambda-2)} \frac{1}{A^{\lambda-2}} , \tag{A.1}$$

$$I_1^\mu \equiv \int_{-\infty}^{+\infty} \ell^\mu \frac{d^4\ell}{[A \pm \ell^2]^\lambda} = 0 , \tag{A.2}$$

$$I_2^{\mu\nu} \equiv \int_{-\infty}^{+\infty} \ell^\mu \ell^\nu \cdot \frac{d^4\ell}{[A \pm \ell^2]^\lambda} = I_0 \left\{ \frac{\pm g^{\mu\nu} \cdot A}{2(\lambda-3)} \right\} , \tag{A.3}$$

$$I_4 \equiv \int_{-\infty}^{+\infty} \ell^4 \frac{d^4\ell}{[A \pm \ell^2]^\lambda} = I_0 \left\{ \frac{6A^2}{(\lambda-3)(\lambda-4)} \right\} . \tag{A.4}$$

We begin with the case of all-scalar particles. The amplitude for diagram (a) then reads

$$T_a = G \cdot \frac{1}{(k - \frac{k'}{2})^2 - m_c^2} \cdot L_a , \tag{A.5}$$

$$L_a \equiv (-\frac{i}{\pi^2}) \cdot \int_{-\infty}^{+\infty} d^4\ell \left\{ \prod_{r=1}^{4} \frac{1}{q_r^2 - m_r^2} \right\} , \tag{A.6}$$

where the internal momenta are defined as in Fig. 4a. In order to perform the loop integration we use the Feynman parameter integral

$$\frac{1}{f_1 \cdots f_N} = (N-1)! \int_0^1 (d\alpha)^N \frac{\delta(1-\Sigma\alpha)}{[\sum_1^N \alpha_r \cdot f_r]^N} , \tag{A.7}$$

which permits evaluation of the loop integration by writing

$$\psi(\alpha,\ell) \equiv \sum_{r=1}^{4} \alpha_r \circ (q_r^2-m_r^2) \equiv A^\circ (\ell-B/A)^2+\left(\frac{AC-B^2}{A}\right) \qquad (A.8)$$

Application of the transformation $\ell' = \ell - B/A$ and use of Eq. (A.7) leads to the result

$$L_a = \int_0^1 (d\alpha)^4 \circ \frac{\delta(1-\Sigma\alpha)}{[D_s]^2} \circ \qquad (A.9)$$

Replacement of all (momenta)^2-factors by the external masses and kinematical variables gives

$$D_s \equiv AC-B^2 = \frac{s}{2}\alpha_1 \circ \alpha_3 + d_s , \qquad (A.10)$$

where the negative definite function

$$d_s = t\circ \alpha_2(\tfrac{1}{2}\alpha_1+\alpha_4) - m_N^2\circ \alpha_3\circ (\tfrac{1}{2}\alpha_1+\alpha_3) - m_c^2\circ \alpha_1(\alpha_1+2\alpha_2+2\alpha_3) - m_G^2\circ(\alpha_2+\alpha_4)\circ(\sum_1^4 \alpha_r) \qquad (A.11)$$

For later use we define

$$d_s^1 \equiv d_s(\alpha_1=0) , \; d_s^3 \equiv d_s(\alpha_3=0) , \; d_s^o \equiv d_s(\alpha_1=\alpha_3=0). \qquad (A.12)$$

At this point we also mention the relation

$$(k-k')^2 - m_c^2 = \frac{1}{2}(t-m_\psi^2) , \qquad (A.13)$$

which when inserted in Eq. (A.5) indicates a t-pole at $t = m_\psi^2$. We have assumed $m_\psi^2 = 4m_c^2$ throughout. Diagram (c) could be calculated in the same way. However, we skip this step by noticing that diagram (c) is obtained from diagram (a) by the replacement $p_1 \leftrightarrow -p_2$. Thus

$$T_c = G \circ \frac{2}{t-m_\psi^2} \circ L_c \qquad (A.14)$$

with

$$L_c = \int_0^1 (d\alpha)^4 \frac{\delta(1-\Sigma\alpha)}{D_u^2} , \tag{A.15}$$

where

$$D_u \equiv -\frac{s}{2}\alpha_1\alpha_3 + d_u \tag{A.16}$$

and

$$d_u = t \circ \left\{\alpha_2(\tfrac{1}{2}\alpha_1+\alpha_4)-\tfrac{1}{2}\alpha_1\alpha_3\right\} + m_N^2\alpha_3(\tfrac{1}{2}\alpha_1-\alpha_3)$$

$$- m_c^2\alpha_1(\alpha_1+2\alpha_2) - m_G^2(\alpha_2+\alpha_4)\left(\sum_1^4 \alpha_r\right) . \tag{A.17}$$

Note that d_u^1, d_u^3, d_u^o, which are defined analogously to Eqs. (A.12) for the s-channel, are identical with d_s^1, d_s^3, d_s^o. All quantities D_s, D_u, d_s, d_u, etc., should actually carry the index (4), $D_s \equiv D_s(4)$..., since they refer to diagrams j = (a,b,c,d) with four internal lines. We have omitted this index in order to simplify our notation. Going through the same procedure with the amplitude for diagram (e) is straightforward and leads to

$$D_s \equiv \frac{s}{2}\alpha_3(\alpha_5-\alpha_1) + d_s , \tag{A.18}$$

where

$$d_s \equiv \frac{t}{2}h_1 - m_N^2 h_2 - m_c^2 h_3 - m_G^2 h_4 \tag{A.19}$$

$$h_1 = \alpha_2(\alpha_4+\alpha_5) + \alpha_4(\alpha_1+\alpha_2) - \alpha_1\alpha_3$$

$$h_2 = \alpha_3\{\alpha_3 - \frac{1}{2}(\alpha_1 - \alpha_5)\}$$

$$h_3 = \alpha_1(\alpha_1+2\alpha_4+2\alpha_5)+\alpha_5(\alpha_5+2\alpha_2+2\alpha_3)$$

$$h_4 = (\alpha_2 + \alpha_4)\left(\sum_1^5 \alpha_r\right) . \tag{A.20}$$

For later convenience we introduce the transformation

$$\bar{\alpha}_1 = \alpha_1 + \alpha_5 , \quad \bar{\alpha}_5 = \alpha_5 - \alpha_1 , \tag{A.21}$$

and newly define:

$$\bar{D}_s = \frac{s}{2} \alpha_3 \bar{\alpha}_5 + \bar{d}_s . \tag{A.22}$$

$\bar{d}_s$ is defined by d_s with α_1 and α_5 replaced according to the above transformation. Furthermore we will need the quantities $\bar{d}_s^1$, $\bar{d}_s^5$, $\bar{d}_s^o$ which are specified as in Eq. (A.12). Similarly we introduce

$$D_u \equiv -\frac{s}{2} \alpha_3 (\alpha_5 - \alpha_1) + d_u \tag{A.23}$$

with

$$d_u \equiv \frac{t}{2} \; h_1 - m_N^2 \, h_2 - m_c^2 \, h_3 - m_G^2 \, h_4 , \tag{A.24}$$

$$h_1 = \alpha_2(\alpha_4 + \alpha_5) + \alpha_4(\alpha_1 + \alpha_2) - \alpha_1 \alpha_3 ,$$

$$h_2 = \alpha_3 \{ \alpha_3 + \frac{1}{2}(\alpha_1 - \alpha_5) \} ,$$

$$h_3 = \alpha_1(\alpha_1 + 2\alpha_3 + 2\alpha_4) + \alpha_5(\alpha_5 + 2\alpha_1 + 2\alpha_2) ,$$

$$h_4 = (\alpha_2 + \alpha_4)\left(\sum_1^5 \alpha_r\right) . \tag{A.25}$$

Note that, again, all quantities D_s ... should actually carry the index (5): $D_s(5)$, ..., since they refer to the diagrams with five internal lines. We have omitted this index for simplicity of notation.

We now evaluate the loop integrals $\not{L}_j$ for spin-$\frac{1}{2}$ c-quarks and spinless gluons; their form is

$$\not{L}_a \equiv \left(-\frac{i}{\pi^2}\right) \int_{-\infty}^{+\infty} d^4\ell \{ -\not{\ell} + m_c \} \left(\prod_{r=1}^{4} \frac{1}{q_r^2 - m_r^2} \right) , \tag{A.26}$$

$$V\!\!\!/_c \equiv \left(-\frac{i}{\pi^2}\right) \int_{-\infty}^{+\infty} d^4\ell \{\ell\!\!\!/ + m_c\} \left(\prod_{r=1}^{4} \frac{1}{q_r^2 - m_r^2} \right), \tag{A.27}$$

$$V\!\!\!/_e \equiv \left(-\frac{i}{2\pi^2}\right) \int_{-\infty}^{+\infty} d^4\ell \{ (\ell\!\!\!/ + m_c) \epsilon\!\!/ (q\!\!\!/_5 + m_c) \} \left(\prod_{r=1}^{5} \frac{1}{q_r^2 - m_r^2} \right). \tag{A.28}$$

The loop integration can be performed as sketched above, with modifications due to the spin factors. In particular we have to remember the linear transformation $\ell' = \ell - B/A$. By use of the integrals, Eqs. (A.1) - (A.4), we find:

$$V\!\!\!/_a = \int_0^1 (d\alpha)^4 \{m_c - x\!\!\!/_1\} \cdot I_a(\alpha). \tag{A.29}$$

Here we introduce the convention

$$x\!\!\!/_1 \equiv -p\!\!\!/_1 \alpha_2 + p\!\!\!/_2(\alpha_2+\alpha_3) + \frac{k\!\!\!/'}{2}(\alpha_2+\alpha_3+\alpha_4), \tag{A.30}$$

$$x\!\!\!/_2 \equiv -p\!\!\!/_1(\alpha_2+\alpha_3) + p\!\!\!/_2 \alpha_2 + \frac{k\!\!\!/'}{2}(\alpha_2+\alpha_3+\alpha_4). \tag{A.31}$$

The same analysis for diagram (c) leads to

$$V\!\!\!/_c = \int_0^1 (d\alpha)^4 \{m_c + x\!\!\!/_2\} \cdot I_c(\alpha). \tag{A.32}$$

The spin factor of diagram (e) is evaluated by dropping all terms linear in ℓ'_μ since their contributions vanish in the loop integration. Using Eqs. (A.1) - (A.4) we obtain

$$V\!\!\!/_e = \left(\frac{-i}{2\pi^2}\right) \int_{-\infty}^{+\infty} d^4\ell \{ (q\!\!\!/_1 + m_c) \epsilon\!\!/ (q\!\!\!/_5 + m_c) \} \left(\prod_{r=1}^{5} \frac{1}{q_r^2 - m_r^2} \right)$$

$$= \int_0^1 (d\alpha)^5 \{ \epsilon\!\!/ \frac{D_e}{2} + (m_c + y\!\!\!/_1) \epsilon\!\!/ (m_c + y\!\!\!/_1 - k\!\!\!/) \} \cdot I_e(s) \tag{A.33}$$

where again we have introduced the convention of writing

$$y\!\!\!/_1 = k\!\!\!/(\alpha_4+\alpha_5) + \frac{k\!\!\!/'}{2}(\alpha_2+\alpha_3-\alpha_4) - p\!\!\!/_1 \alpha_3 \tag{A.34}$$

$$\not{v}_2 = \not{k}(\alpha_3+\alpha_4+\alpha_5) + \frac{\not{k}'}{2}(\alpha_2-\alpha_3-\alpha_4) + \not{p}_1\alpha_3 \,. \tag{A.35}$$

Using the rule

$$\begin{aligned} \not{I}_b &= \not{I}_a(p_1 \to -p_2) \,, \\ \not{I}_d &= \not{I}_c(p_1 \leftrightarrow -p_2) \,, \\ \not{I}_f &= \not{I}_e(p_1 \leftrightarrow -p_2) \,, \end{aligned} \tag{A.36}$$

one easily establishes the spin factors for diagrams (b), (d), and (f), as given in Eqs. (3.13) and (3.14). For simplicity of notation we sometimes use the simplifying convention that, instead of writing the index of each diagram in $I_j(\alpha)$, we will rather use s or u in agreement with D_s or D_u of the particular diagram. The generalization of the above formalism to amplitudes describing spin-$\frac{1}{2}$ c-quarks which interact via spin-1 gluons with the spinless nucleon is straightforward; we therefore only indicate modifications.

In the integrands of Eqs. (A.26) - (A.28) for $\not{I}_j$, the spin parts differ. We first consider diagram (a). The curly bracket in $\not{I}_a$ of Eq. (A.26) is replaced by

$$\{(\not{p}_1+\not{q}_3)(-\not{\ell}+m_c)(\not{q}_3+\not{p}_2)\} \,. \tag{A.37}$$

We now follow the same procedure as above: replacement of all internal momenta by the external ones, replacement $\ell = \ell'+B$ and subsequent rearrangement of terms as follows:

$$\begin{aligned} \{\ldots\} &= (\not{p}_1+\not{p}_2+\not{p}_4-\not{x}_1-\not{\ell}')(m_c-\not{x}_1-\not{\ell}')(2\not{p}_2+\not{p}_4-\not{x}_1-\not{\ell}') \equiv (\not{v}_1-\not{\ell}')(\not{v}_2-\not{\ell}')(\not{v}_3-\not{\ell}') \\ &= \{\not{v}_1\not{v}_2\not{v}_3 + \ell'^2\cdot(\not{v}_1+\not{v}_3) + \not{\ell}'\not{v}_2\not{\ell}'\} + \{\text{terms with odd powers of } \ell'\} \,. \end{aligned} \tag{A.38}$$

We have defined

$$\begin{aligned} \not{v}_1 &\equiv \qquad (\not{p}_1a_1 + \not{p}_2b_1 + \not{k}'c_1) \,, \\ \not{v}_2 &\equiv m_c + (\not{p}_1a_2 + \not{p}_2b_2 + \not{k}'c_2) \,, \end{aligned}$$

$$\not{v}_3 \equiv (\not{p}_1 a_3 + \not{p}_2 b_3 + \not{k}' c_3) \; , \tag{A.39}$$

where the $a_i, \ldots$, etc., depend linearly on the integration parameters α. Inserting the definition of $\not{x}_1$, given in Eq. (A.30/31), into Eq. (A.38) defines the expansion coefficients in terms of the integration parameters α:

$$\begin{aligned}
a_1 &= 1 + \alpha_2 \; , & b_1 &= 1 - \alpha_2 - \alpha_3 \; , & c_1 &= \tfrac{1}{2}\alpha_1 \; , \\
a_2 &= \alpha_2 \; , & b_2 &= -(\alpha_2 + \alpha_3) \; , & c_2 &= -\tfrac{1}{2}(1-\alpha_1) , \\
a_3 &= \alpha_2 \; , & b_3 &= 2 - (\alpha_2 + \alpha_3) , & c_3 &= \tfrac{1}{2}\alpha_1 \; .
\end{aligned} \tag{A.40}$$

Using the integration formulas in Eqs. (A.1) - (A.4) in order to perform the $d^4\ell$ integration, one finds

$$\not{S}_a \equiv \not{v}_1 \not{v}_2 \not{v}_3 + 2\, D_s (\not{v}_1 + \not{v}_3) + \tfrac{1}{2}\, D_s \gamma_\mu \not{v}_2 \gamma^\mu \tag{A.41}$$

We now consider the modifications in diagram (c) due to spin–1 gluon exchange. The curly bracket in the integrand of Eq. (A.27) is replaced by

$$\{ (\not{p}_1 - \not{q}_3)(\not{\ell} + m_c)(\not{p}_2 - \not{q}_3) \} \; . \tag{A.42}$$

In principle we now could go through all modifications as before. In the explicit evaluation of the helicity matrix elements, however, we found it more convenient to take advantage of the relation $\not{V}_c = -\not{V}_a(p_1 \leftrightarrow -p_2,\; m_c \to -m_c)$. This therefore leads to $\not{S}_c = -\not{S}_a(w_i)$ with

$$\begin{aligned}
\not{w}_1 &\equiv \qquad\quad (-\not{p}_2 a_1 - \not{p}_1 b_1 + \not{k}' c_1) \; , \\
\not{w}_2 &\equiv - m_c + (-\not{p}_2 a_2 - \not{p}_1 b_2 + \not{k}' c_2) \; , \\
\not{w}_3 &\equiv \qquad\quad (-\not{p}_2 a_3 - \not{p}_1 b_3 + \not{k}' c_3) \; .
\end{aligned} \tag{A.43}$$

All $a_i \ldots$ are chosen as for diagram (a) and are specified in Eqs. (A.40).

The spin factors for diagrams (b) and (d) are determined by the replacement $p_1 \leftrightarrow -p_2$ in those of diagrams (a) and (c). This does not modify the form of $\not{S}_a$

as a function of the $\not v_i$; however, it does change the expansion coefficients $a_i \ldots$ (as functions of the integration parameters α) in the $\not v_i$ according to:

$$
\begin{aligned}
a_1 &= -1 + (\alpha_2 + \alpha_3)\ , & b_1 &= -(1+\alpha_2)\ , & c_1 &= \tfrac{1}{2}\alpha_1\ , \\
a_2 &= (\alpha_2 + \alpha_3)\ , & b_2 &= -\alpha_2\ , & c_2 &= -\tfrac{1}{2}(1-\alpha_1)\ , \\
a_3 &= -2 + (\alpha_2 + \alpha_3)\ , & b_3 &= -\alpha_2\ , & c_3 &= \tfrac{1}{2}\alpha_1\ . \qquad \text{(A.44)}
\end{aligned}
$$

To summarize, all spin factors $\not S_a, \ldots, \not S_d$ are given by Eq. (3.34) as a function of the v_i (w_i). Differences in the spin factors arise in the expansion coefficients of these quantities. $a_i \ldots$ for diagrams (a) and (c) are given in Eq. (A.40), whereas the ones for diagrams (b) and (d) are given in Eq. (A.44).

We now determine the spin factors of diagrams (e) and (f). The curly bracket in the integrand of $\not V_e$ in Eq. (A.28) is replaced by

$$\{ (\not p_1 + \not q_3)(\not q_1 + m_c)\not e (\not q_5 + m_c)(\not q_3 + \not p_2) \}\ , \qquad \text{(A.45)}$$

which, by writing the internal momenta in terms of the external momenta and the loop momentum $\not \ell'$, may be cast into the form:

$$\{\ldots\} \equiv (\not v_1 + \not \ell')(m_c + \not v_2 + \not \ell')\not e (m_c + \not v_3 + \not \ell')(\not v_4 + \not \ell') \qquad \text{(A.46)}$$

where

$$\not v_i \equiv \not p_1 \ a_i + \not k \ b_i + \not k' \ c_i \quad (i = 1, \ldots, 4)\ . \qquad \text{(A.47)}$$

The curly bracket is expanded in $\not \ell'$ and the $d^4\ell$ integration is performed using Eqs. (A.1) – (A.4). All terms with an odd number of $\not \ell'$ vanish upon integration, leading to

$$\not S_e \equiv \not S_{e_1} + \not S_{e_2} + \not S_{e_3} \qquad \text{(A.48)}$$

whose explicit forms are given in Eqs. (3.45) – (3.47).

The same reasoning for diagram (f) leads to $\not S_f \equiv \not S_e(v_i)$ and the two expressions differ only in the expansion coefficients v_i as a function of the integration parameters α. The coefficients in the v_i are easily evaluated and we find for diagram (e):

$$
\begin{aligned}
&a_1 = 2-\alpha_3 , \quad b_1 = \alpha_4 + \alpha_5 , \quad c_1 = \tfrac{1}{2}(\alpha_2+\alpha_3-\alpha_4-1) , \\
&a_2 = -\alpha_3 , \quad b_2 = \alpha_4 + \alpha_5 , \quad c_2 = \tfrac{1}{2}(\alpha_2+\alpha_3-\alpha_4) , \\
&a_3 = -\alpha_3 , \quad b_3 = \alpha_4+\alpha_5-1 , \quad c_3 = \tfrac{1}{2}(\alpha_2+\alpha_3-\alpha_4) , \\
&a_4 = 2-\alpha_3 , \quad b_4 = \alpha_4+\alpha_5+1 , \quad c_4 = \tfrac{1}{2}(\alpha_2+\alpha_3-\alpha_4-3) ,
\end{aligned}
\tag{A.49}
$$

and for diagram (f):

$$
\begin{aligned}
&a_1 = \alpha_3-2 , \quad b_1 = \alpha_3+\alpha_4+\alpha_5-2 , \quad c_1 = \tfrac{1}{2}(\alpha_2-\alpha_3-\alpha_4+3), \\
&a_2 = \alpha_3 , \quad b_2 = \alpha_3+\alpha_4+\alpha_5 , \quad c_2 = \tfrac{1}{2}(\alpha_2-\alpha_3-\alpha_4) , \\
&a_3 = \alpha_3 , \quad b_3 = \alpha_3+\alpha_4+\alpha_5-1 , \quad c_3 = \tfrac{1}{2}(\alpha_2-\alpha_3-\alpha_4) , \\
&a_4 = \alpha_3-2 , \quad b_4 = \alpha_3+\alpha_4+\alpha_5-1 , \quad c_4 = \tfrac{1}{2}(\alpha_2-\alpha_3-\alpha_4+1) .
\end{aligned}
\tag{A.50}
$$

APPENDIX B

Here we give details of the "spin amplitudes" Q_i, defined in Eq. (3.18) and (3.23). In order to clarify our notation, we define the momenta and wave-functions.

The momentum 4-vectors in the CM-system are:

$$k^{\mu} = (k, 0, 0, k), \quad k'^{\mu} = (E', k' \sin\theta, 0, k' \cos\theta), \tag{B.1}$$

$$p_1^{\mu} = (E_1, 0, 0, -k), \quad p_2^{\mu} = (E_2, -k' \sin\theta, 0, -k' \cos\theta) . \tag{B.2}$$

We have used the following spin 1/2 wave functions:

$$u_+ = \begin{bmatrix} F_+ \cos\frac{\theta}{2} \\ F_+ \sin\frac{\theta}{2} \\ F_- \cos\frac{\theta}{2} \\ F_- \sin\frac{\theta}{2} \end{bmatrix}, \quad u_- = \begin{bmatrix} -F_+ \sin\frac{\theta}{2} \\ F_+ \cos\frac{\theta}{2} \\ F_- \sin\frac{\theta}{2} \\ -F_- \cos\frac{\theta}{2} \end{bmatrix}, \quad F_\pm = \sqrt{\frac{\frac{1}{2} E' + m_c}{2 m_c}},$$

$$v_+ = \begin{bmatrix} F_- \sin\frac{\theta}{2} \\ -F_- \cos\frac{\theta}{2} \\ -F_+ \sin\frac{\theta}{2} \\ F_+ \cos\frac{\theta}{2} \end{bmatrix}, \quad v_- = \begin{bmatrix} -F_- \cos\frac{\theta}{2} \\ -F_- \sin\frac{\theta}{2} \\ -F_+ \cos\frac{\theta}{2} \\ -F_+ \sin\frac{\theta}{2} \end{bmatrix}, \tag{B.3}$$

and the photon polarization vectors read:

$$\epsilon_\pm = \frac{1}{\sqrt{2}} \begin{bmatrix} 0 \\ \mp 1 \\ -i \\ 0 \end{bmatrix} . \tag{B.4}$$

We comment about the definition of our spinors. Since the $c\bar{c}$-state describes a particle of spin-1, we have chosen the phase convention of the spinors in agreement with the phase of the spin-1 helicity polarization of a particle moving in the direction $\vec{k}'(\theta)$. This demands that in constructing the $\bar{c}$-spinor v_1, the antiquark has to be considered as a 2-state in the sense of Jacob and Wick,[10] which finally results in the change:

$$v_\lambda \to (-1)^{\frac{1}{2}-\lambda} \cdot v_\lambda . \tag{B.5}$$

The spinors in Eq. (B.3) have been obtained by a simple boost and rotation θ and do not contain this change. The above phase convention, however, has been taken into account in the matrix elements, Eqs. (3.18) and (3.23).

The calculation of the "spin amplitudes":

$$\langle\lambda_1\lambda_2|Q_i|\lambda_\gamma = +1\rangle \equiv Q_i(\lambda_1\lambda_2) \tag{B.6}$$

is straightforward and we therefore list here only a few examples

$$\begin{aligned}
Q_1(++) &= -\sqrt{8}\cos^2\frac{\theta}{2}k[(E_1+k)+2k'\sin^2\frac{\theta}{2}] && \overset{s\to\infty}{\Longrightarrow} -\sqrt{2}(s-m_N^2) , \\
Q_1(-+) &= \sin\theta\left(\frac{1}{m_c}\right)[E_1(E'k-E_1k)+E'k^2(1-\frac{k'}{k}\cos\theta)] && \Longrightarrow \frac{\sqrt{-t}}{m_c}(-\frac{t}{2}+4m_c^2) , \\
Q_1(--) &= -\sqrt{8}\sin^2\frac{\theta}{2}k[(E_1+k)-2k'\cos^2\frac{\theta}{2}] && \Longrightarrow -\sqrt{2}\,\frac{t}{s}(t-4m_c^2+m_N^2) ,
\end{aligned} \tag{B.7}$$

and so on.

APPENDIX C

Here we list the expansion coefficients $\xi, \eta, \zeta, \ldots$, in the amplitudes $M_j(p, \alpha)$ in Eqs. (3.38) and (3.39):

$$
\begin{aligned}
\underline{M_a}: \quad \xi_1 &= + \frac{1}{\sqrt{8}} (1-\alpha_1)(2-\alpha_3)^2 , \\
\eta_1 &= - \frac{\sqrt{2}}{16} (1-\alpha_1)(2-\alpha_3)^2 , \\
\zeta_1 &= - \frac{\sqrt{2}}{8} (4\alpha_1 - \alpha_1\alpha_3 + \alpha_1^2\alpha_3) ,
\end{aligned} \tag{C.1}
$$

$$
\begin{aligned}
\underline{M_b}: \quad \xi_1 &= + \frac{1}{\sqrt{8}} (1-\alpha_1)(2-\alpha_3)^2 , \\
\eta_1 &= - \frac{\sqrt{2}}{16} (1-\alpha_1)(2-\alpha_3)^2 , \\
\zeta_1 &= + \frac{\sqrt{2}}{8} (4\alpha_1 - \alpha_1\alpha_3 + \alpha_3\alpha_1^2) ,
\end{aligned} \tag{C.2}
$$

$$
\begin{aligned}
\underline{M_c}: \quad \xi_1 &= + \frac{1}{\sqrt{8}} (1-\alpha_1)(2-\alpha_3)^2 , \\
\eta_1 &= + \frac{\sqrt{2}}{16} (1-\alpha_1)(2-\alpha_3)^2 , \\
\zeta_1 &= + \frac{\sqrt{2}}{8} \alpha_1\alpha_3(1-\alpha_1) ,
\end{aligned} \tag{C.3}
$$

$$
\begin{aligned}
\underline{M_d}: \quad \xi_1 &= + \frac{1}{\sqrt{8}} (1-\alpha_1)(2-\alpha_3)^2 , \\
\eta_1 &= + \frac{\sqrt{2}}{16} (1-\alpha_1)(2-\alpha_3)^2 , \\
\zeta_1 &= - \frac{\sqrt{2}}{8} \alpha_1\alpha_3(1-\alpha_1) .
\end{aligned} \tag{C.4}
$$

The phase convention Eq. (B.5) for the v-spinor has been taken into account. The expansion coefficients (ξ_5, η_5, ζ_5) in Eq. (3.44) hide a $\ln^2(-s)$ dependence; their explicit forms are:

$$
\begin{aligned}
\underline{M_a}: \quad \xi_5 &= 3\alpha_3 - 8 , & \underline{M_b}: \quad \xi_5 &= -3\alpha_3 + 8 , \\
\eta_5 &= -3\alpha_3 + 8 , & \eta_5 &= 3\alpha_3 - 8 , \\
\zeta_5 &= \tfrac{1}{2}(3\alpha_1 - 1) , & \zeta_5 &= \tfrac{1}{2}(3\alpha_1 - 1) ,
\end{aligned} \tag{C.5,6}
$$

$$\underline{M_c}:\ \xi_5 = 3\alpha_3 - 8\,, \qquad \underline{M_d}:\ \xi_5 = -3\alpha_3 + 8\,,$$

$$\eta_5 = 3\alpha_3 - 8\,, \qquad \eta_5 = -3\alpha_3 + 8\,,$$

$$\zeta_5 = \tfrac{1}{2}(3\alpha_1 - 1)\,, \qquad \zeta_5 = \tfrac{1}{2}(3\alpha_1 - 1)\,. \tag{C.7,8}$$

The expansion coefficients appearing in the amplitudes of the nonplanar diagrams (e) and (f) are:

$$\underline{M_{e_1}}:\ \xi_1 = \frac{1}{\sqrt{2}}[(2-\alpha_3)(1-\alpha_2-\alpha_3-\alpha_4-2\alpha_5)]\,,$$

$$\eta_1 = \frac{\sqrt{2}}{4}[(2-\alpha_3)(\alpha_4+\alpha_5)]\,,$$

$$\zeta_1 = \frac{\sqrt{2}}{4}[1+\{1+2\alpha_4+2\alpha_5\}\{2+\alpha_2-\alpha_3-\alpha_4\}]\,, \tag{C.9}$$

$$\underline{M_{e_2}}:\ \xi_1 = -\frac{\sqrt{2}}{4}(2-\alpha_3)^2\,,$$

$$\eta_1 = +\frac{\sqrt{2}}{4}[(2-\alpha_3)(3+\alpha_2-\alpha_3-\alpha_4)]\,,$$

$$\zeta_1 = +\frac{\sqrt{2}}{8}[(2-\alpha_3)(\alpha_2+\alpha_3-\alpha_4)]\,, \tag{C.10}$$

$$\underline{M_{e_3}}:\ \xi_1 = \frac{\sqrt{2}}{4}\alpha_3[\alpha_3^3+\alpha_3^2\cdot A_2+\alpha_3\cdot A_1+A_0]\,,$$

$$A_0 \equiv -2(1-\alpha_2-\alpha_4-2\alpha_5)^2\,,$$

$$\eta_1 = -\frac{\sqrt{2}}{16}[\alpha_3^4+\alpha_3^3\cdot A_3+\alpha_3^2\cdot A_2+\alpha_3\cdot A_1+A_0]\,,$$

$$A_0 \equiv 4\{(\alpha_2^2-\alpha_4^2)+2(\alpha_5-1)(\alpha_2-\alpha_4)\}\,,$$

$$\zeta_1 = -\frac{\sqrt{2}}{8}[\alpha_3^4\cdot A_4+\alpha_3^3\cdot A_3+\alpha_3^2\cdot A_2+\alpha_3\cdot A_1+A_0]\,,$$

$$A_0 \equiv \{4(\alpha_2^2-\alpha_4^2)+(8\alpha_5-2)(\alpha_2-\alpha_4)\}\,, \tag{C.11}$$

$$\underline{M_{f_1}}:\ \xi_1 = -\frac{1}{\sqrt{2}}[(2-\alpha_3)(1-\alpha_2-\alpha_3-\alpha_4-2\alpha_5)]\,,$$

$$\eta_1 = +\frac{\sqrt{2}}{4}\,[(2-\alpha_3)(2-\alpha_3-\alpha_4-\alpha_5)]\ ,$$

$$\zeta_1 = +\frac{\sqrt{2}}{4}\,[1+\{2-\alpha_2-\alpha_3+\alpha_4\}\{3-2\alpha_3-2\alpha_4-2\alpha_5\}]\ , \qquad \text{(C.12)}$$

$\underline{M_{f_2}}$:

$$\xi_1 = -\frac{\sqrt{2}}{4}(2-\alpha_3)^2\ ,$$

$$\eta_1 = +\frac{\sqrt{2}}{4}\,[(2-\alpha_3)(1-\alpha_2-\alpha_3+\alpha_4)]\ ,$$

$$\zeta_1 = -\frac{\sqrt{2}}{8}\,[(2-\alpha_3)(\alpha_2-\alpha_3-\alpha_4)]\ , \qquad \text{(C.13)}$$

$\underline{M_{f_3}}$:

$$\xi_1 = -\frac{\sqrt{2}}{4}\,\alpha_3\,[\alpha_3^3+\alpha_3^2\cdot A_2+\alpha_3\cdot A_1+A_0]\ ,$$

$$A_0 \equiv -2(1-\alpha_2-\alpha_4-2\alpha_5)^2\ ,$$

$$\eta_1 = -\frac{\sqrt{2}}{16}\cdot[\alpha_3^4+\alpha_3^3\cdot A_3+\alpha_3^2\cdot A_2+\alpha_3\cdot A_1+A_0]\ ,$$

$$A_0 \equiv 4\{(\alpha_2^2-\alpha_4^2)+2(\alpha_5-1)(\alpha_2-\alpha_4)\}\ ,$$

$$\zeta_1 = -\frac{\sqrt{2}}{8}\,[\alpha_3^4\cdot A_4+\alpha_3^3\cdot A_3+\alpha_3^2\cdot A_2+\alpha_3\cdot A_1+A_0]\ ,$$

$$A_0 \equiv \{4(\alpha_2^2-\alpha_4^2)+(8\alpha_5-6)(\alpha_2-\alpha_4)\}\ . \qquad \text{(C.14)}$$

REFERENCES

1. B. Humpert and A.C.D. Wright, Phys. Lett. 65B, 463 (1976).
2. B. Humpert and A.C.D. Wright, "Spin and mass dependence of models for ψ photoproduction," Stanford Linear Accelerator Center preprint SLAC-PUB-1818 (1976), to be published in Phys. Rev. D.
3. D. Gross and F. Wilczek, Phys. Rev. Lett. 30, 1343 (1973); H. Politzer, Phys. Rev. Lett. 30, 1346 (1973).
4. F. E. Low, Phys. Rev. D 12, 163 (1975); S. Nussinov, Phys. Rev. Lett. 34, 1286 (1975); Phys. Rev. D 14, 246 (1976).
5. T. Appelquist and H. D. Politzer, Phys. Rev. Lett. 34, 43 (1975).
6. J. D. Bjorken and S. D. Drell, Relativistic Quantum Mechanics (McGraw-Hill Book Co., New York, 1965).
7. R. J. Eden et al., The Analytic S-Matrix (Cambridge University Press, New York, 1966), p. 151.
8. Ibid., p. 133.
9. J. Ballam et al., Phys. Rev. D 7, 3150 (1973); Phys. Rev. D 5, 545 (1972); Phys. Rev. Lett. 24, 960 (1970).
10. M. Jacob and G. C. Wick, Ann. Phys. (N.Y.) 7, 404 (1959).

FIGURE CAPTIONS

1. Lepton decay of the photoproduced ψ-resonance.
2. ψ-photoproduction in a picture of quarks interacting via gluons.
3. Photoproduction of $\psi \equiv (c\bar{c})$ as viewed in a two-gluon exchange model.
4. Integration region for integral (4.54).
5. Size and t-dependence of residue functions $f_t(\xi)$ appearing in the asymptotic form of the amplitudes of diagrams (a) - (d).
6. Size and t-dependence of residue functions $h_t(\xi)$ appearing in the asymptotic form of the amplitudes of diagrams (e) and (f).
7. m_G-dependence of residue functions $f_t(1)$ (Eq. (3.51)) and $h_t(1)$ (Eq. (3.58)). This behavior is representative of all integrals of the same type.
8. m_V-dependence of residue functions f_t and h_t given in Eqs. (3.51) and (3.58).
9. Two-gluon exchange model with vector gluons. Density matrix element ρ^0_{00} for ρ- and ψ-photoproduction as a function of the gluon mass m_G in the region where the nonflip amplitude vanishes (peak). The kinematical variables are $s = 30\ \mathrm{GeV}^2$, $t = -0.2\ (\mathrm{GeV}/c)^2$.
10. Two-gluon exchange model with vector gluons. Density matrix element ρ^0_{00} for ρ- and ψ-photoproduction as a function of the gluon mass m_G in the region where the nonflip amplitude vanishes (peak). The kinematical variables are $s = 30\ \mathrm{GeV}^2$, $t = -2.0\ (\mathrm{GeV}/c)^2$.
11. Position of the peak (in Fig. 9) as a function of m_V and m_G for $s = 30\ \mathrm{GeV}^2$ and $t = -0.2\ (\mathrm{GeV}/c)^2$.
12. Two-gluon exchange model with vector gluons. Gluon mass dependence and relative size of the flip and nonflip amplitudes (in arbitrary units) for ψ-photoproduction. The kinematical variables are $s = 30\ \mathrm{GeV}^2$, $t = -0.2(\mathrm{GeV}/c)^2$.
13. Two-gluon exchange model with vector gluons. Gluon mass dependence of

the nonflip amplitude for ψ-photoproduction. The amplitudes of diagrams (a) - (d) and diagrams (e) and (f) are presented separately. The kinematical variables are $s = 30\ \mathrm{GeV}^2$, $t = -0.2\ (\mathrm{GeV/c})^2$.

14. Two-gluon exchange model with vector gluons. t-dependence of ρ^0_{00} for ρ-photoproduction at the peak. The gluon mass was chosen to be $m_G = 0.04$ GeV.

15. Two-gluon exchange model with vector gluons. t-dependence of ρ^0_{00} for ψ-photoproduction at the peak. The gluon mass was chosen to be $m_G =$ 1.0 GeV.

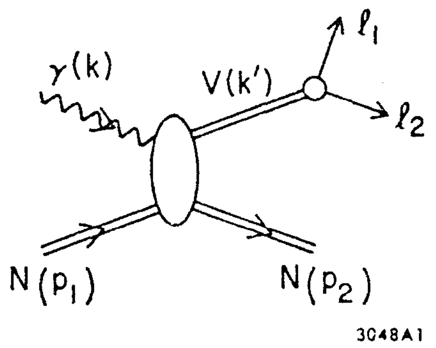

Fig. 1

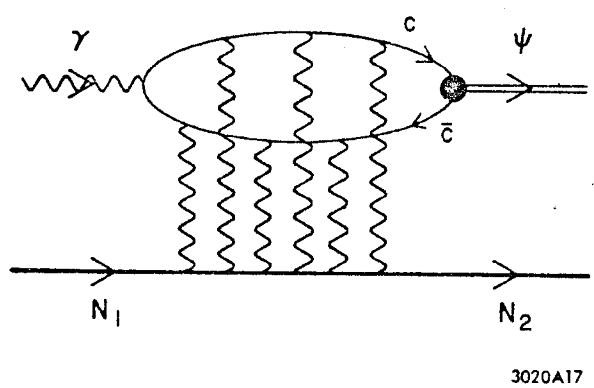

Fig. 2

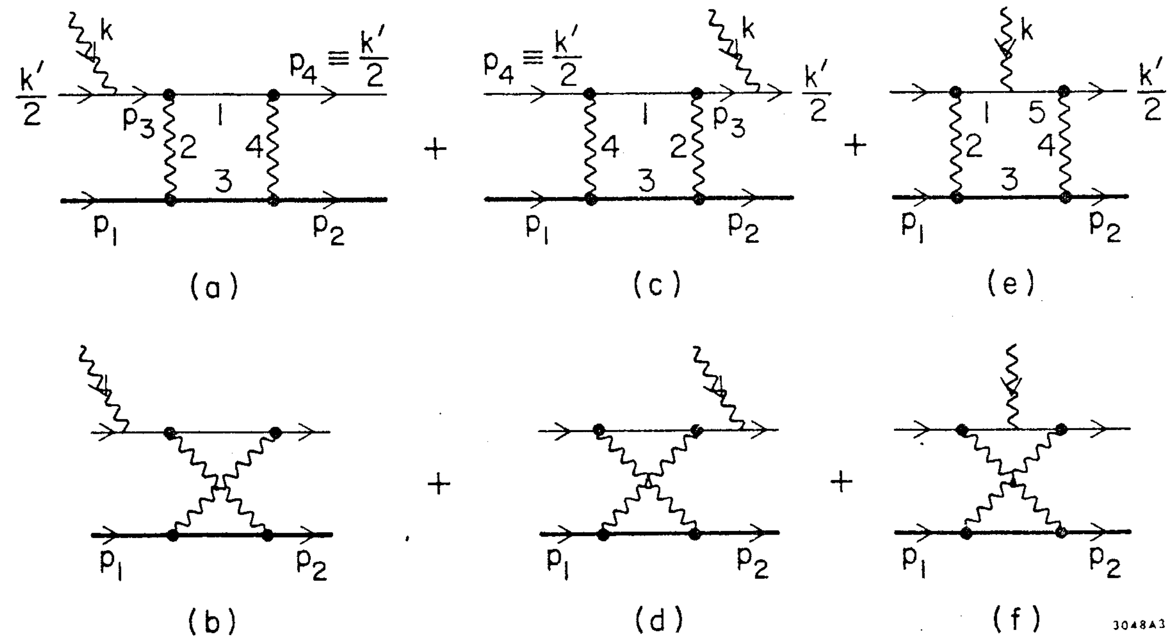
k
$\frac{k'}{2}$
p_3
$p_4 \equiv \frac{k'}{2}$
1
2
3
4
p_1
p_2
(a)
+
$p_4 \equiv \frac{k'}{2}$
k
p_3
$\frac{k'}{2}$
(c)
+
k
5
(e)
(b)
(d)
(f)
3048A3

Fig. 3

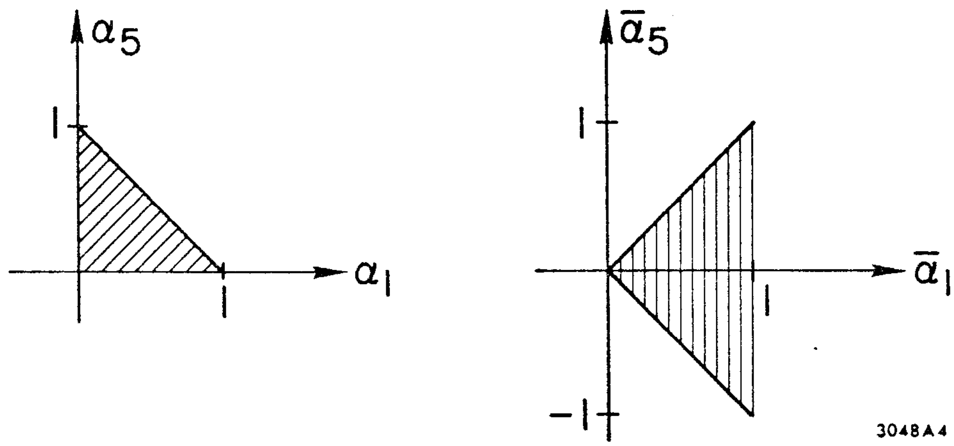

Fig. 4

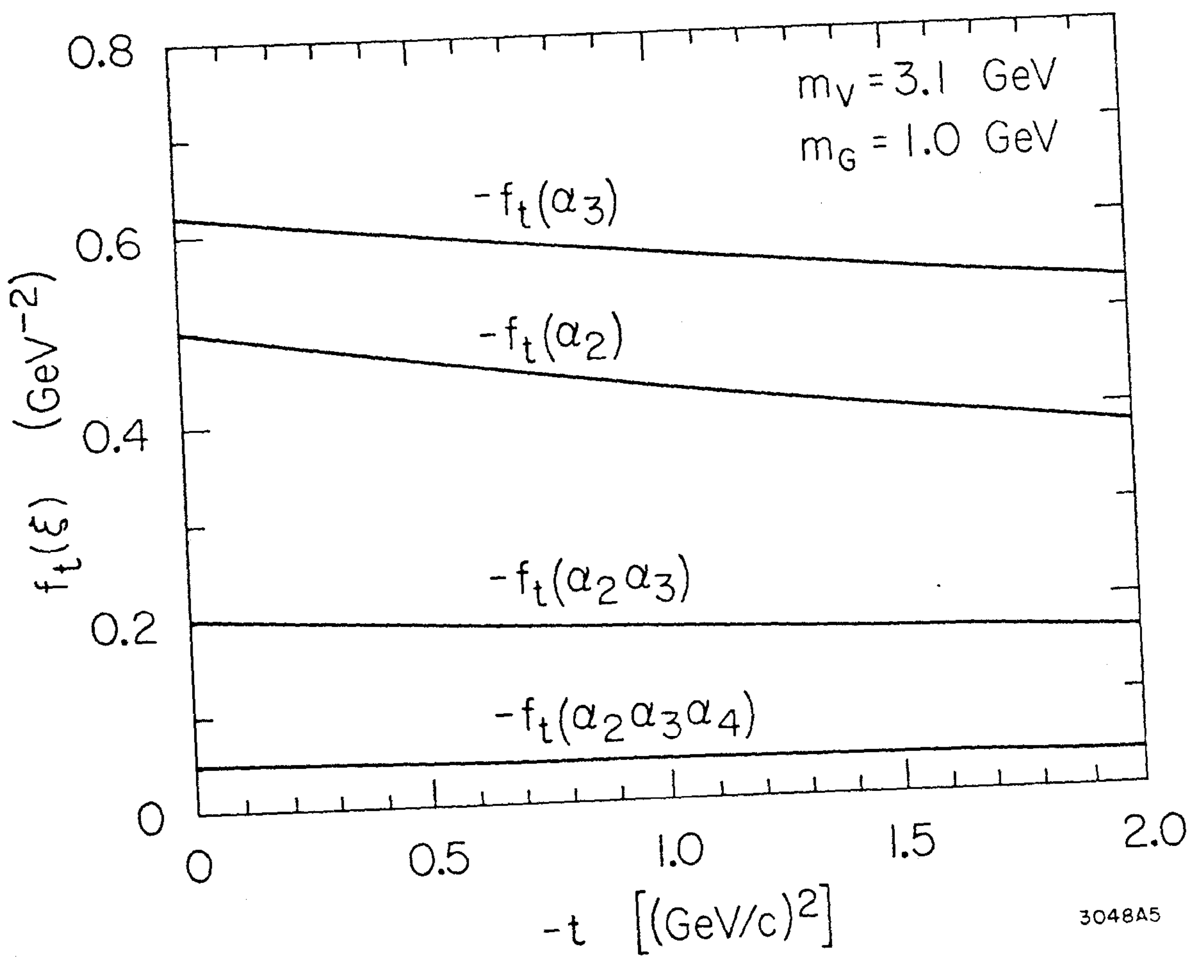

$m_V = 3.1$ GeV
$m_G = 1.0$ GeV
$-f_t(\alpha_3)$
$-f_t(\alpha_2)$
$-f_t(\alpha_2\alpha_3)$
$-f_t(\alpha_2\alpha_3\alpha_4)$
$f_t(\xi)$ (GeV^{-2})
0.8
0.6
0.4
0.2
0
0
0.5
1.0
1.5
2.0
$-t$ $[(\mathrm{GeV}/c)^2]$
3048A5

Fig. 5

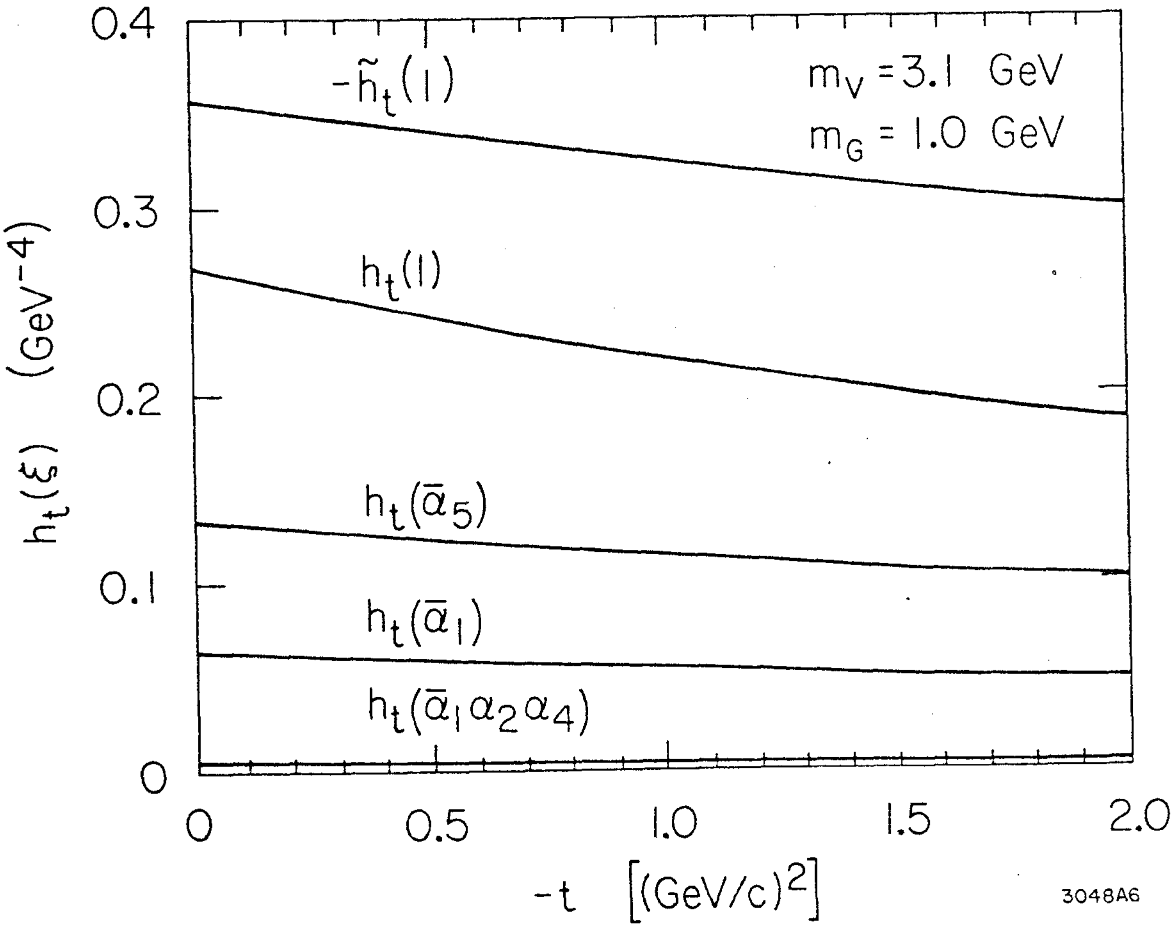

0.4
0.3
0.2
0.1
0
$h_t(\xi)$ (GeV^{-4})
$-\tilde{h}_t(1)$
$h_t(1)$
$h_t(\bar{\alpha}_5)$
$h_t(\bar{\alpha}_1)$
$h_t(\bar{\alpha}_1\alpha_2\alpha_4)$
$m_V = 3.1$ GeV
$m_G = 1.0$ GeV
0
0.5
1.0
1.5
2.0
$-t$ $[(\mathrm{GeV}/c)^2]$
3048A6

Fig. 6

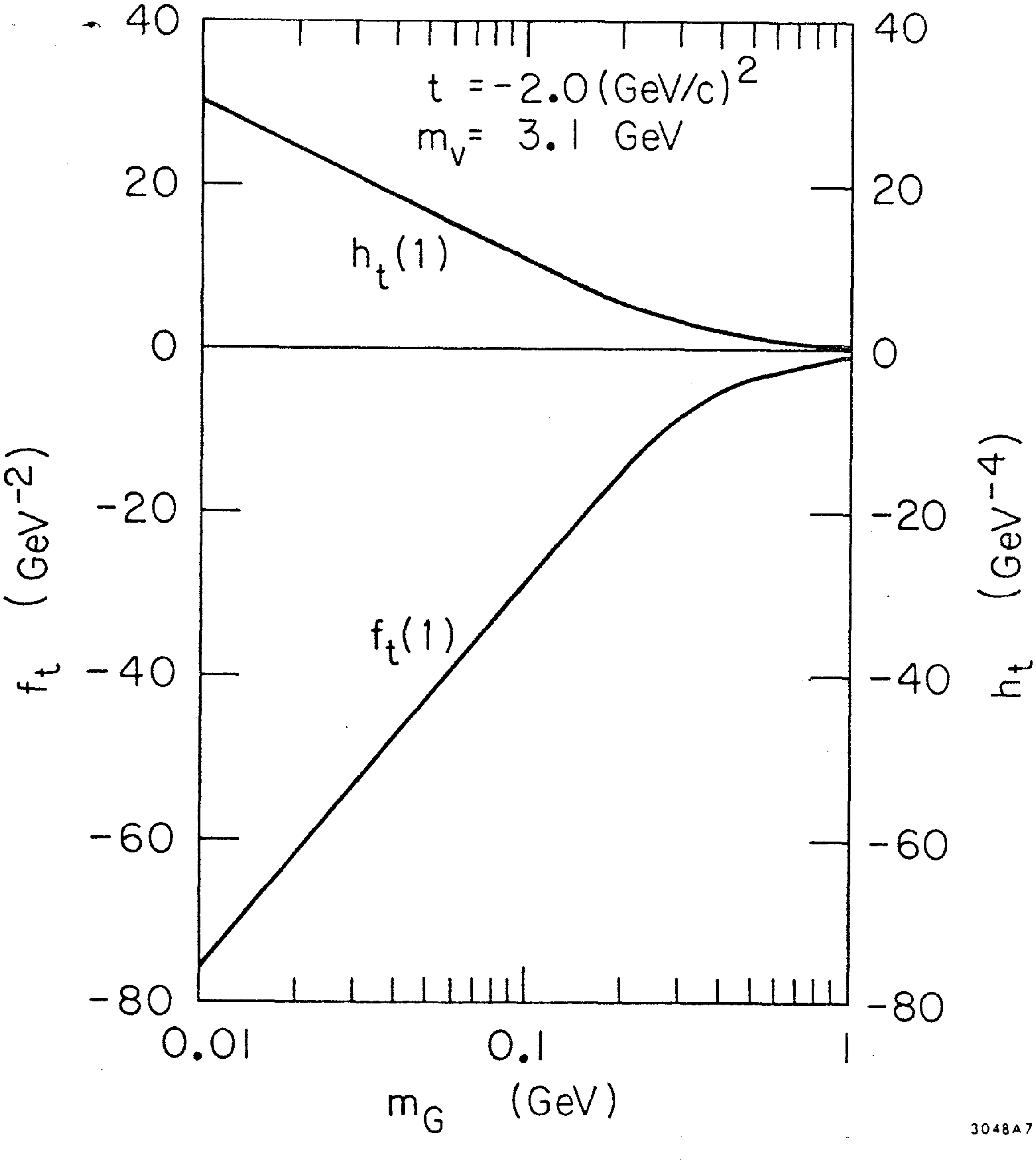

40
20
0
-20
-40
-60
-80
f_t (GeV^{-2})
40
20
0
-20
-40
-60
-80
h_t (GeV^{-4})
t = -2.0 (GeV/c)^2
m_V = 3.1 GeV
$h_t(1)$
$f_t(1)$
0.01
0.1
1
m_G (GeV)
3048A7

Fig. 7

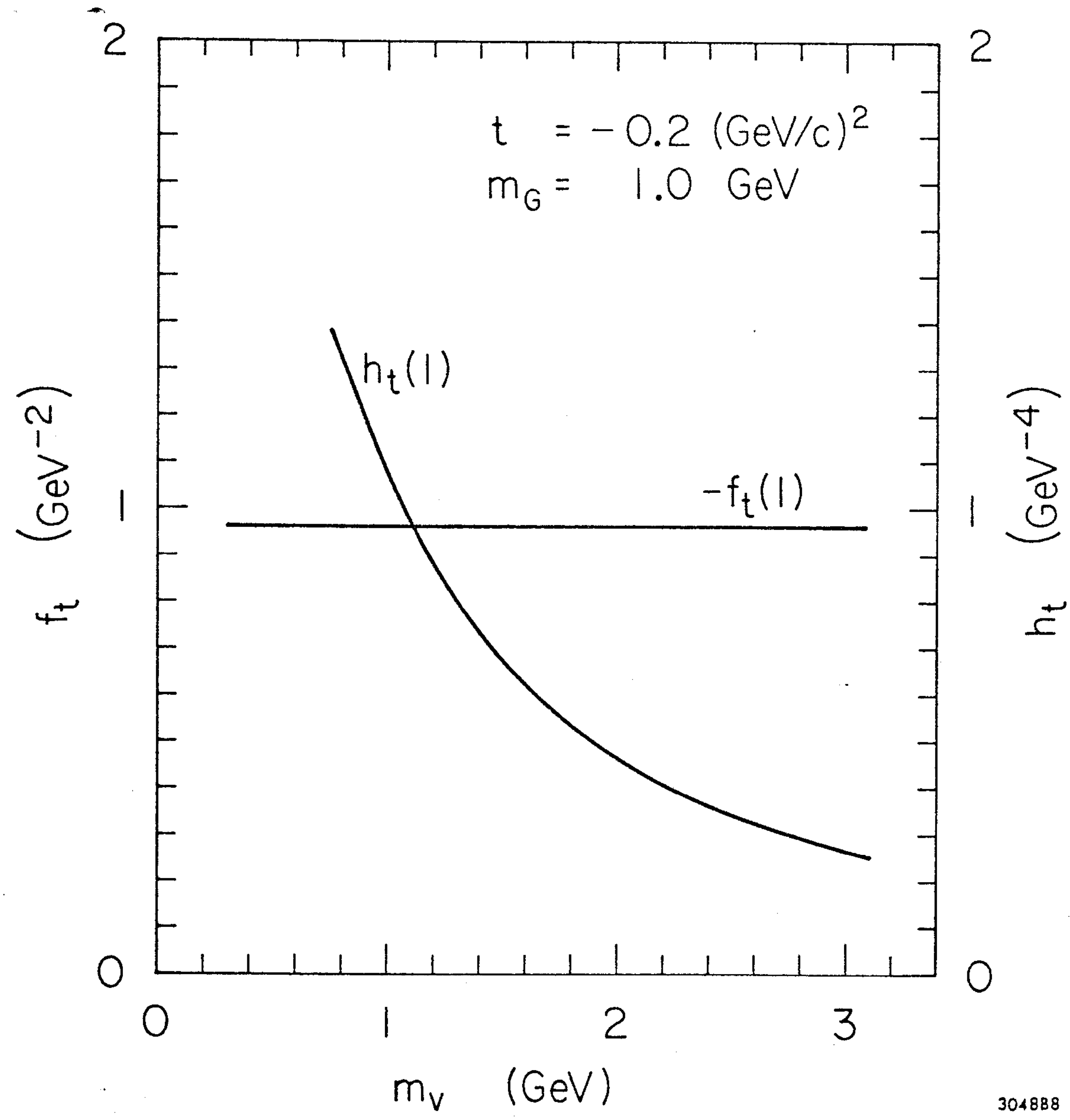

Fig. 8

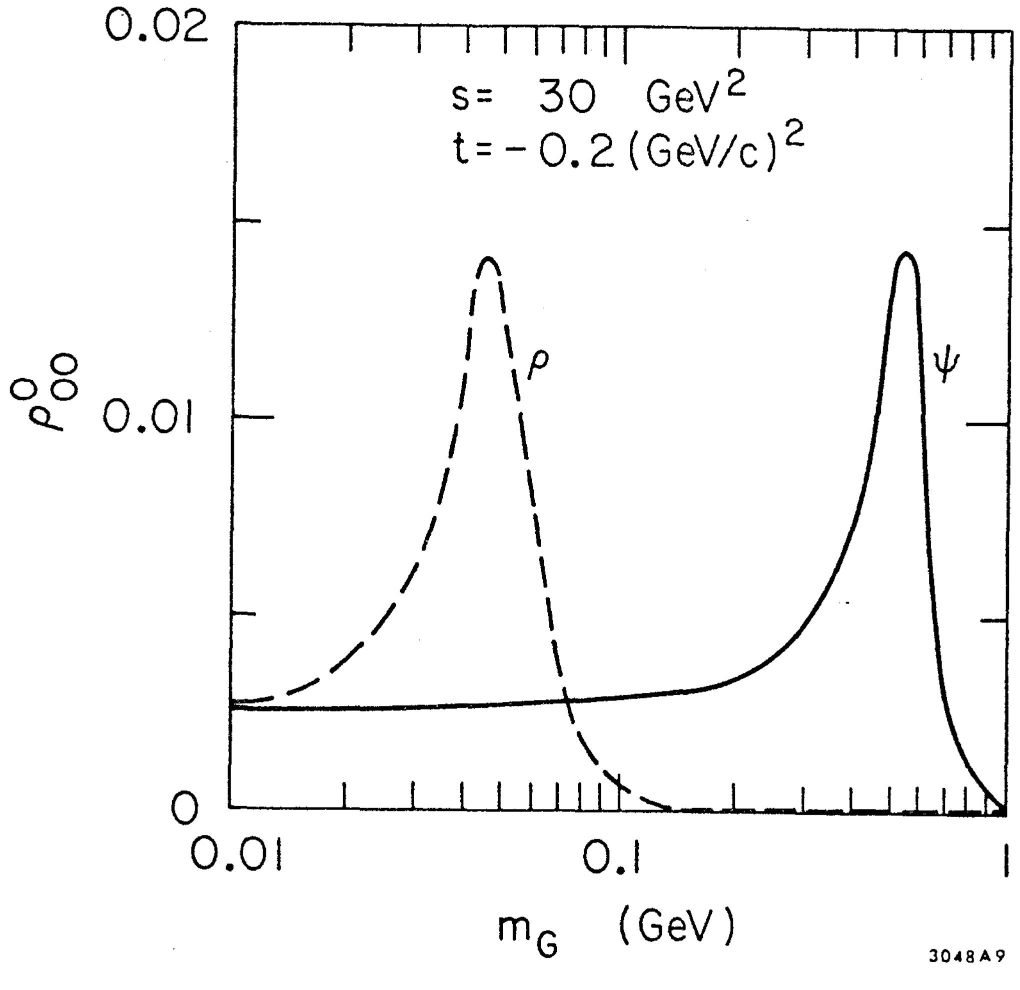

0.02
s= 30 GeV^2
t=-0.2 (GeV/c)^2
ρ
ψ
ρ^0_{00}
0.01
0
0.01
0.1
1
m_G (GeV)
3048A9

Fig. 9

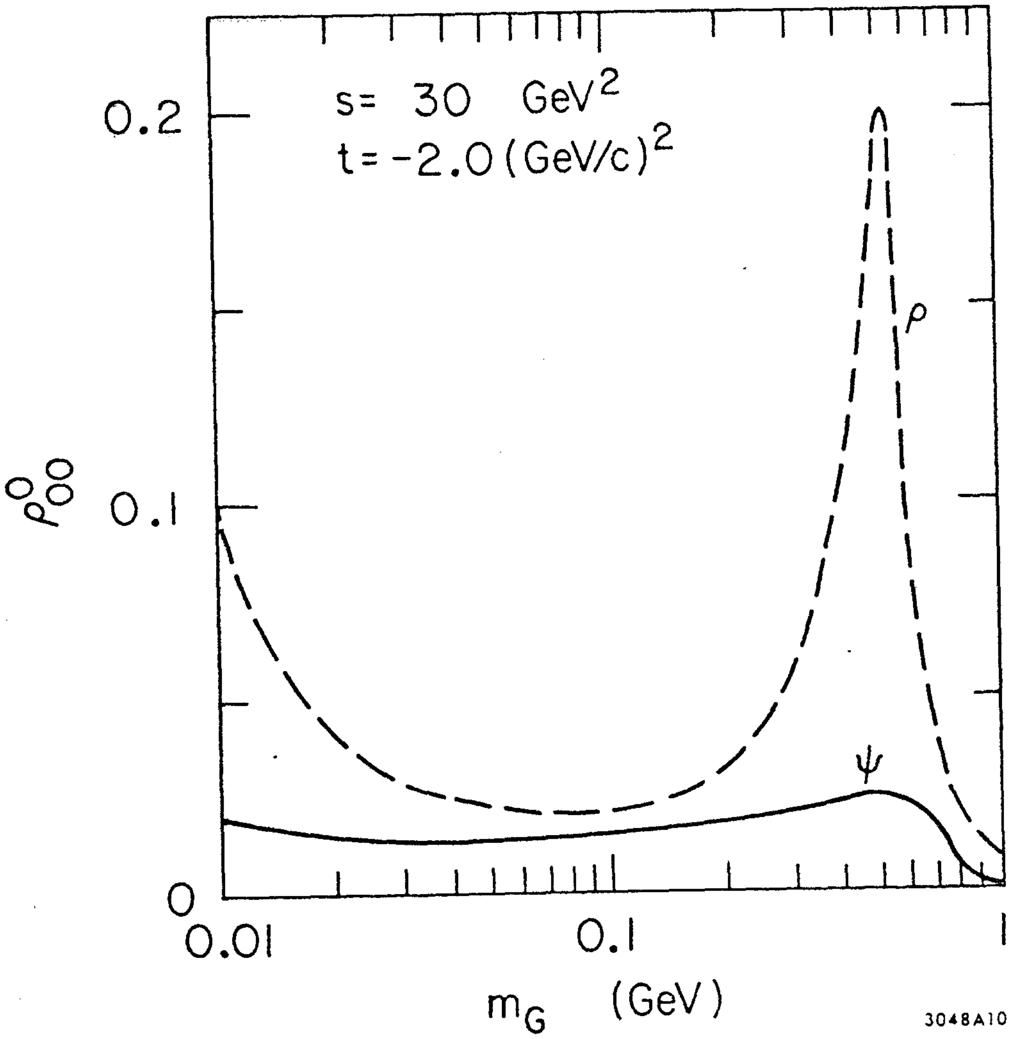

s= 30 GeV^2
t=-2.0(GeV/c)^2
0.2
0.1
0
ρ^0_{00}
ρ
ψ
0.01
0.1
1
m_G (GeV)
3048A10

Fig. 10

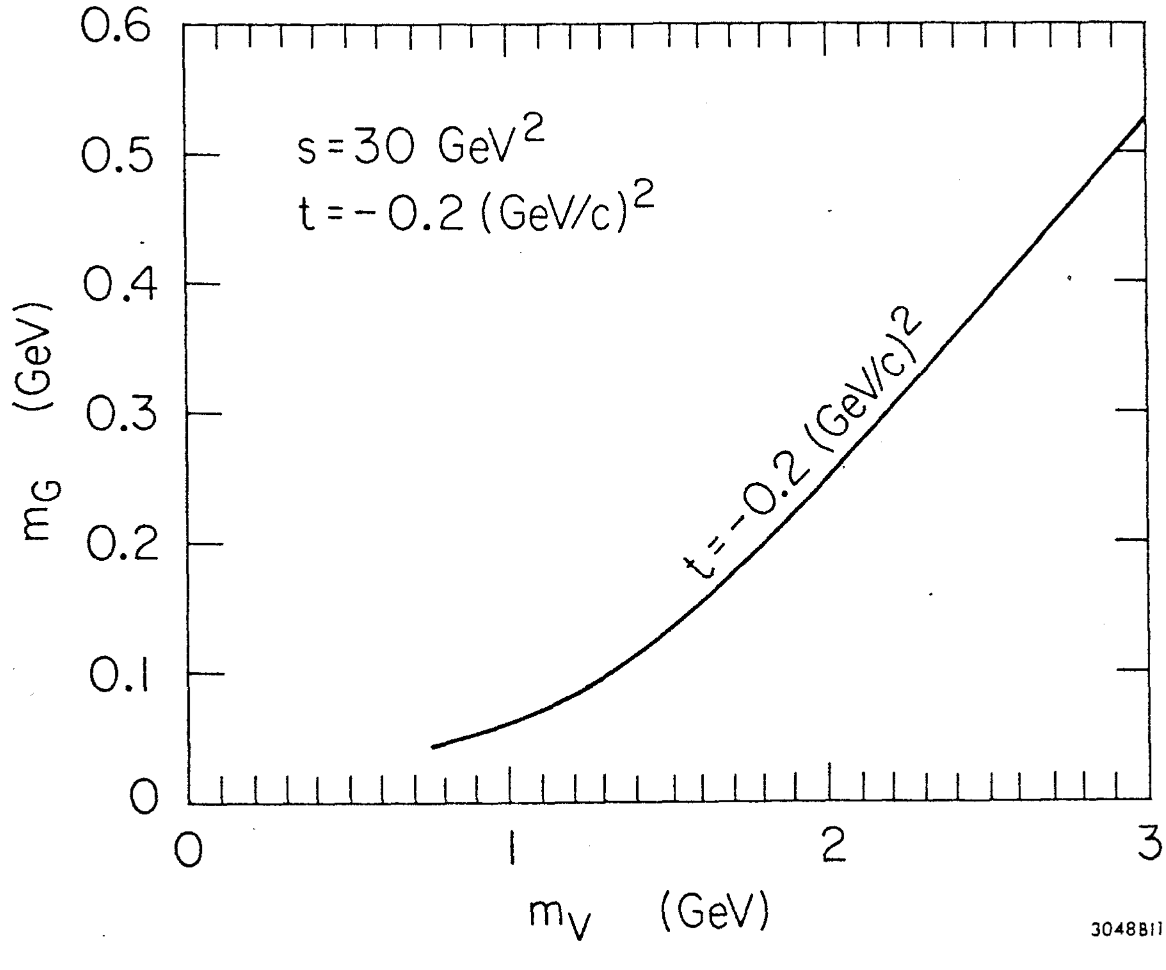
0.6
0.5
0.4
0.3
0.2
0.1
0
s = 30 GeV²
t = −0.2 (GeV/c)²
t = −0.2 (GeV/c)²
m_G (GeV)
0
1
2
3
m_V (GeV)
3048B11

Fig. 11

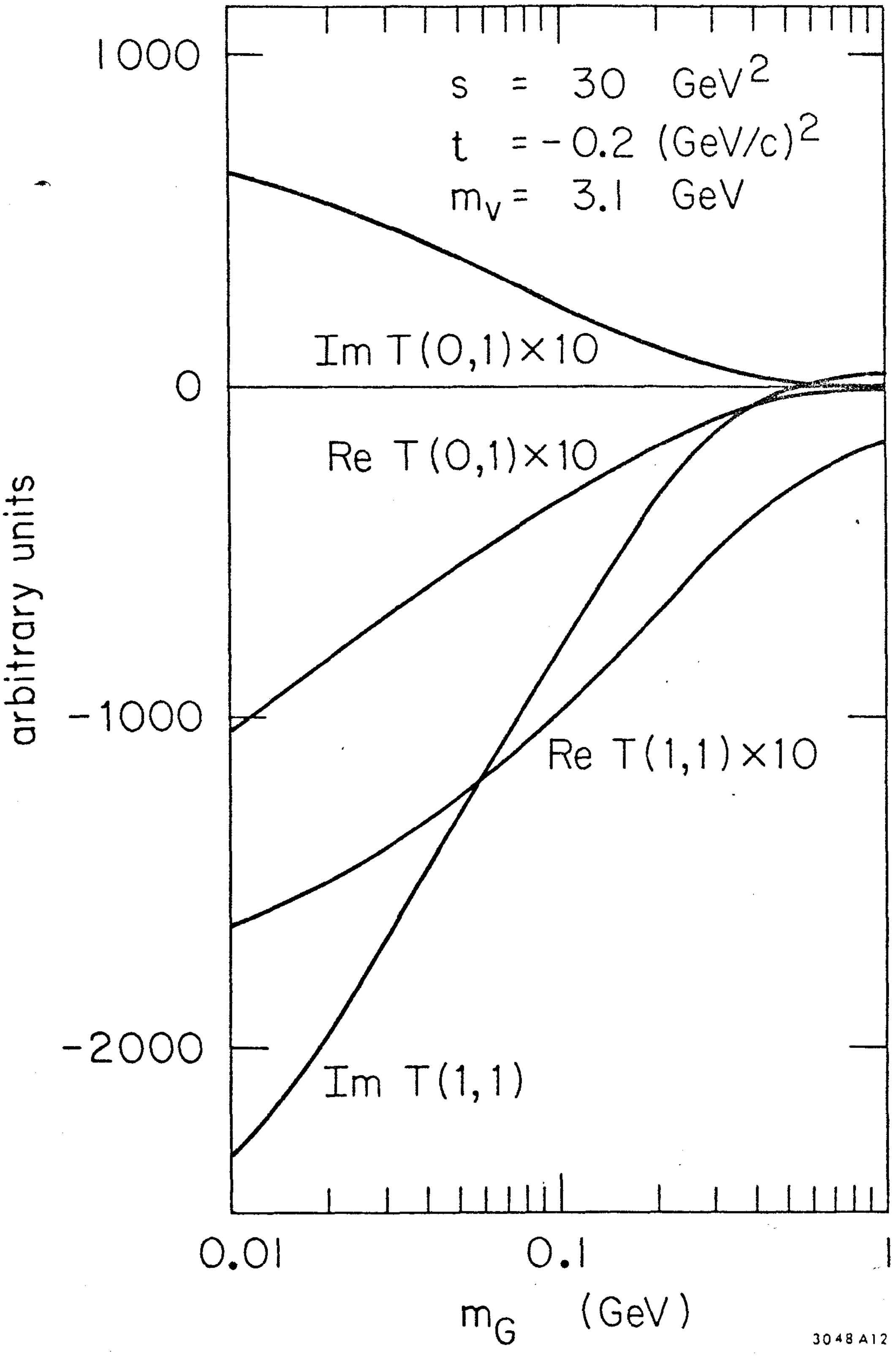

1000
0
-1000
-2000
arbitrary units
s = 30 GeV^2
t = -0.2 (GeV/c)^2
m_V = 3.1 GeV
Im T(0,1)×10
Re T(0,1)×10
Re T(1,1)×10
Im T(1,1)
0.01
0.1
1
m_G (GeV)
3048A12

Fig. 12

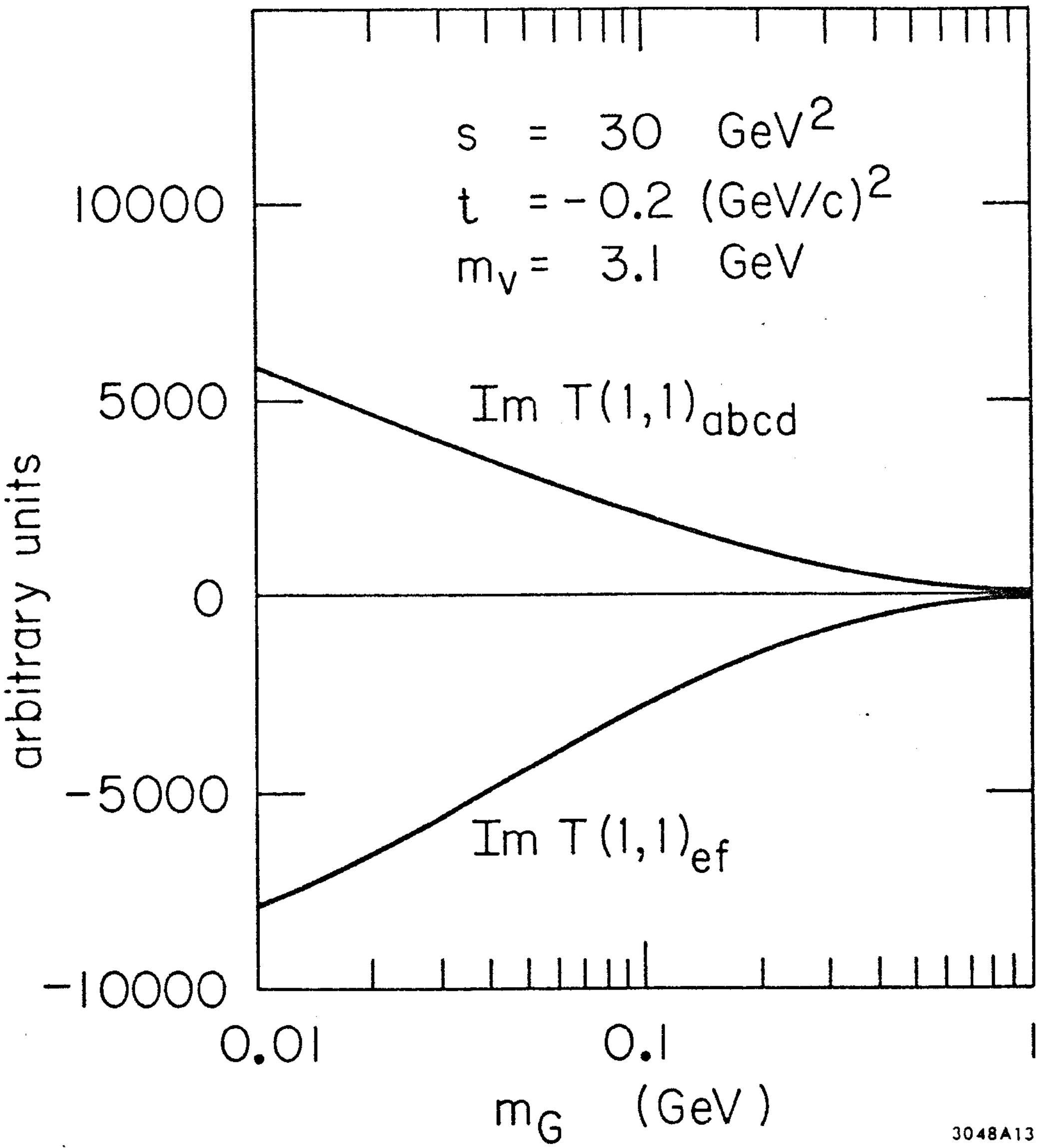
s = 30 GeV^2
t = −0.2 (GeV/c)^2
m_V = 3.1 GeV
Im T(1,1)$_{abcd}$
Im T(1,1)$_{ef}$
10000
5000
0
−5000
−10000
arbitrary units
0.01
0.1
1
m_G (GeV)
3048A13

Fig. 13

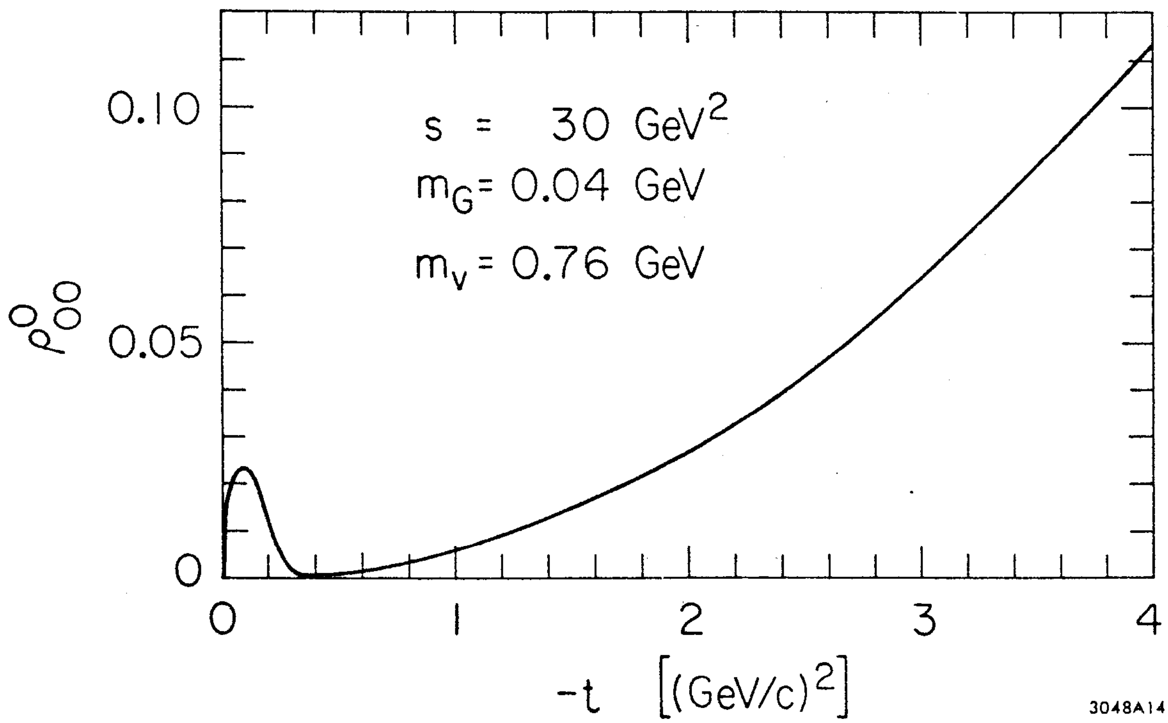

s = 30 GeV²
m_G = 0.04 GeV
m_V = 0.76 GeV
ρ⁰₀₀
0.10
0.05
0
0
1
2
3
4
−t [(GeV/c)²]
3048A14

Fig. 14

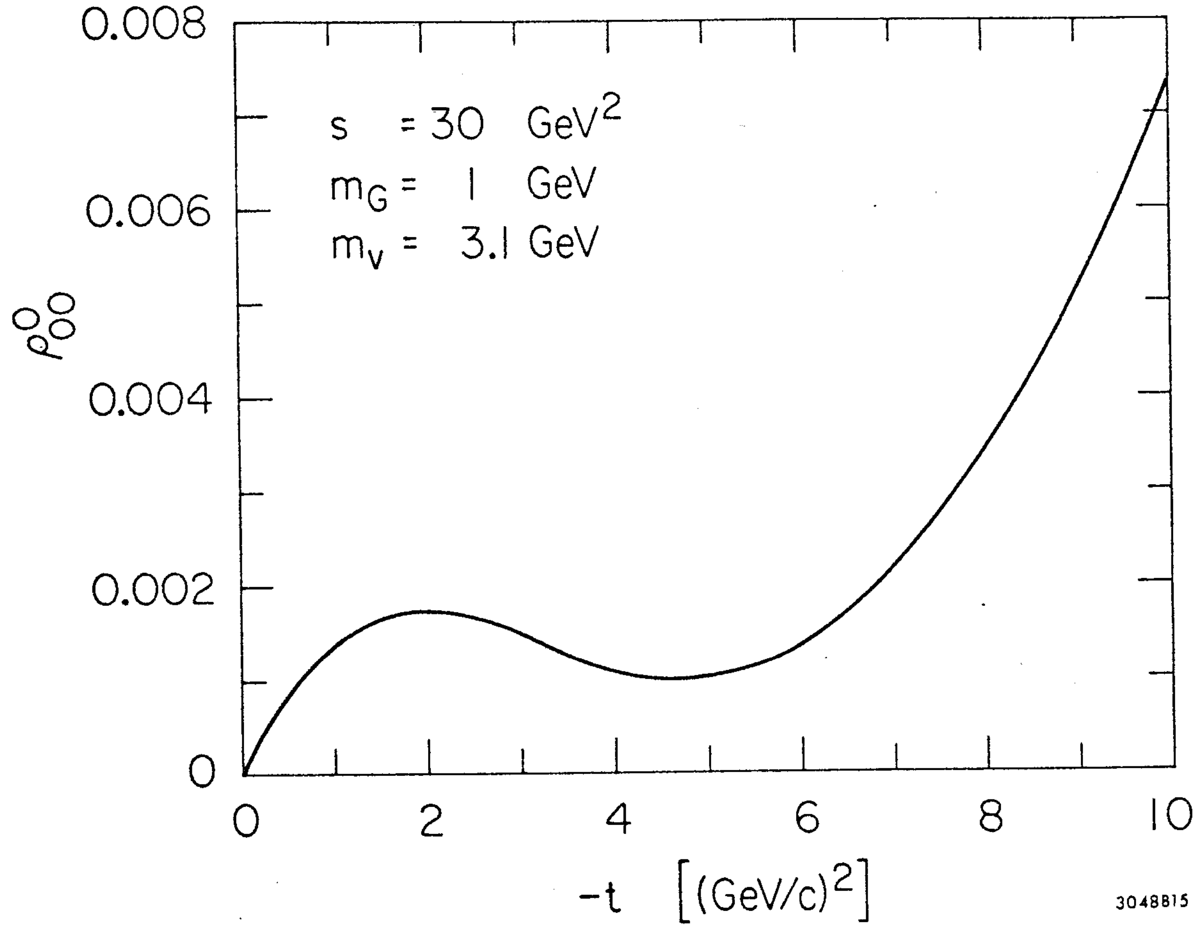
0.008
0.006
0.004
0.002
0
ρ^0_{00}
s = 30 GeV^2
m_G = 1 GeV
m_V = 3.1 GeV
0
2
4
6
8
10
$-t$ [(GeV/c)^2]
3048B15

Fig. 15